Inertial Aerosol Deposition in Neonatal Infant Nasal Airways

by

Scott E. Tavernini

A thesis submitted in partial fulfillment of the requirements for the degree of

Master of Science

Department of Mechanical Engineering

University of Alberta

Abstract

The inertial filtration properties of neonatal infant nasal airways are the focus of this thesis. Nasal replicas based on computed tomography (CT) scan images of seven infants between the ages of 5 and 79 days were created using three-dimensional printing. Deposition of inertial sized aerosol particles in these models was measured using an electrical low pressure impactor (ELPI). The aerosol entering the nasal replica is characterized with the ELPI by sampling through a blank line. The reduction in concentration of aerosol after passing through the nasal replica is the deposited fraction. The ELPI bin geometric centres were used as a single particle size for deposition data. Deposition was recorded for particles with aerodynamic diameters between 0.53 and 5.54 μm. A filtration efficiency correlation was developed through non-linear least squares fitting. This correlation collapsed intersubject variability in the data onto a single curve capable of describing deposition in all the nasal replicas studied. A non-dimensional pressure drop, the Euler number, was required as an input variable in addition to the Reynolds and Stokes numbers to achieve satisfactory collapse of the data. These dimensionless parameters were evaluated with a characteristic dimension defined as the nasal airway volume divided by its surface area. An analysis of expected in-vivo intersubject variability of aerosol filtration was also performed. Further, the ability to scale a previously developed idealized infant nasal airway to produce a model which mimics nasal filtration in the neonatal population was explored. Inertial deposition in three scaled models of the original full scale geometry was measured using the same method used to quantify deposition in the nasal replica models. Comparison of deposition in the scaled idealized models to deposition in the replica models led to the identification of the appropriate scale factor. Non-linear least squares fitting produced a correlation which uses Reynolds and Stokes numbers to describe deposition in this geometry for all scales considered. It is hoped that the results of this thesis will aid future research into aerosol devices specifically for neonatal infants and their unique extrathoracic airways.

Preface

The body chapters of this thesis are presented in a manuscript style, in the same style that they have been submitted to peer reviewed journals for publication. At the time of submitting this thesis they remain under review. Ethics approval from the University of Alberta Research Ethics Board was obtained for the acquisition of CT scan data used in Chapter 2. The ethics submission study title was "Acquisition of Upper and Central Airway Geometries of Neonatal Infants from CT images for use in Investigation of Aerosol Deposition", No. 52637, January 12, 2015. Chapter 2 is a co-authored work for which I am the primary author. I was responsible for the development of the nasal replica models, construction of a testing apparatus and subsequent measurements using that apparatus, analysis of the measurement data, and drafting of the manuscript. Chapter 3 is also a co-authored manuscript for which I am the primary author. I was responsible for scaling previously developed models and measuring deposition in these models using the same apparatus developed in Chapter 2. I was again responsible for analysis of the data and drafting of the manuscript. The co-authors aided me in these endeavours with their expert opinions and editing of the draft manuscripts.

For Meghan, and our future.

Acknowledgements

Completing this project has not been without significant support from friends, family, and colleagues. Without their support this project would have been at the very least magnified in difficulty, or, more likely, completely insurmountable.

My academic supervisor, Dr. Warren Finlay: Without your support and encouragement I would not have started this endeavour. It was you who saw my potential and extended the opportunity to study and research in a world class environment. Your style of supervision provided me an atmosphere to work freely, to make my own research decisions and discoveries, and to manage this project in my own style. Even with so much freedom I never felt alone or without direction, you were always welcoming when I stopped by your office to discuss issues I was facing, and happy to point me towards success. Your frequent visits to the lab provided ample opportunity for me to confirm or correct my understanding and to maintain steady progress. I consider myself very lucky to have studied with a world-renowned researcher such as yourself. Thank you for this magnificent opportunity, your mentorship, and guidance.

Also, Dr. Andrew Martin: Your consultation has provided great clarity to my work. You were also very welcoming when I would pop in to your office to ask a research question, I enjoyed the discussions which followed when one question frequently turned into several. These reinforced my understanding of my work and helped me to formulate meaningful connections between observations. Thank you for your mentorship and editorial support in drafting my manuscripts.

Essential to this project are the replicas of infant nasal cavities in which I have measured deposition. Dr. Michelle Noga: thank you for identifying suitable CT data sets for this project and making them available to me including ensuring this was done with approval from the University of Alberta Research Ethics Board. Also, thank you for your support in scanning the replicas to ensure accuracy. Development of the airway models based on these CT scan data sets was facilitated by the Institute for Reconstructive Sciences in Medicine, specifically Andrew Grosvenor and Heather Logan. Andrew and Heather: thank you for welcoming me into your lab space, providing me direction in reading and segmenting CT data, and extending your expertise in designing models suitable for additive manufacturing methods. Construction of the model replicas was done in the Department of Mechanical Engineering's machine shop; I would like to specifically thank Andrew Campbell, Tuula Hilvo, Marc Maccagno, and Roger Marchand for aiding in construction of the airway models and for providing consultation with your vast technical expertise. Your continuous support certainly eliminated numerous obstacles from my research.

Vital to research projects is space to conduct them. I was extremely lucky to have a lab full of wonderful people who made the occasionally long hours spent in the lab seemingly brief. Helena Orszanska: If it weren't for you I am sure I would still be in the lab trying to get those ELPI plates clean! Your enthusiasm and passion made the lab a very bright space and have reminded me to slow down and appreciate the finer things in life. Your support in experiments, lab procedures, literature review, and general advice regarding graduate studies has been paramount. I cannot thank you enough for all you have done. And all the researchers who have been a part of the Aerosol Research Laboratory, the friendships we have built have made this work extremely enjoyable. The atmosphere of our lab has been one of comradery and community and has been very conducive to success. I have enjoyed working with all of you and wish you success in all your ventures. Conor Ruzycki: I appreciate and value all the fruitful discussions we have had, technical and otherwise. Milad Kiaee: your numerical and computational intellect baffles me, thanks for your help in these aspects. Alvin Ly: your humour and friendship brighten the lab, keep working on those crossovers! And, John Chen: thanks for helping me get started and for being so flexible sharing lab equipment.

The people who got me here and keep me going. Mom and Dad: You have instilled in me a curiosity that, as I am sure you know, keeps me asking- why? It is this curiosity that drives me to learn perpetually. For my entire life you have shown me to take pride in my work, to do my best no matter the triviality of a task, and to always act with integrity. I have been extremely fortunate to have such strong role models in my life. For every opportunity you have afforded me, I thank you in the only way I can and that is to make you proud. And my sister, Jen: your work ethic and determination have been constant sources of motivation for me in this project.

The one this is all for, my best friend and partner, Meghan. You are the only person who truly knew when I struggled and always had the right words to relieve my stress allowing me to return to my work rejuvenated. Your love and encouragement is the ultimate fuel for me. Thank you for your patience throughout this project and listening intently to my long-winded explanations of what I was working on that day. Entering this endeavour was a jump into the unknown which we have navigated together beautifully; I will confidently plunge into any abyss with you knowing we will figure it out together. I cannot wait to see where life takes us next.

Finally, I am thankful for the generous financial support provided by Chiesi Ltd., the Natural Sciences and Engineering Research Council of Canada, and the University of Alberta.

Contents

List of Tables

List of Figures

Chapter 1: Introduction

1.1 Background

Inhaled aerosols have been used by humans to provide therapeutic effects for millennia. The earliest known account of which is an Egyptian papyrus scroll from ~1554 BC describing the inhalation of the vapours of the black henbane plant placed on hot bricks (Stein and Thiel 2017). This was prescribed to alleviate difficulties in breathing. Science, technology, and medicine have evolved immensely and aerosols for inhalation are now specialized formulations that are available in portable, discrete delivery devices. Our ability to identify and manufacture therapeutic agents, and to understand their pharmacodynamics, has allowed us to develop highly effective inhalation therapies which provide targeted delivery of drugs to the lungs. For these therapies to be effective the aerosol particles must reach the lungs, extrathoracic filtration directly influences the dose delivered to the lungs and thus the efficacy of aerosol treatments. Conversely, atmospheric aerosols such as smoke and dust are filtered by the extrathoracic airways thereby protecting the delicate tissues of the lungs. Therefore, a complete understanding of aerosol deposition in the extrathoracic region is required to develop appropriate air quality and particulate matter exposure guidelines in addition to effective therapeutic aerosol treatments.

The extrathoracic airway is commonly defined as all airways inclusive of the nasal and oral entrances to the proximal part of the trachea, depending on the route of inhalation inhaled aerosols will interact with different structures. For nasal breathing, the nasal cavity represents the entrance to the respiratory system; it serves multiple purposes including conditioning air on its way to the lungs by humidifying the air and removing suspended particulate matter. Inhaled air and entrained particles enter the nose through the nostrils into the nasal vestibules where, in adults, numerous hairs act as a coarse filter. These hairs are absent in infants. These two cavities remain divided by the nasal septum until mixing together at the nasopharynx. While the left and right nasal cavities are not symmetrical they roughly mirror each other with the same basic structure. Posterior to the nasal vestibule a constriction of the passage accelerates the flow; this constriction is the point of minimum cross-sectional area and is termed the nasal valve. The passage then expands and the inhaled air encounters three protrusions of mucous covered tissue called conchae, or turbinates (superior, middle, and inferior). The pathway below each turbinate is termed a (superior, middle, or inferior) meatus. The turbinates disrupt and mix the flow through the meatuses and are thought to contribute to inertial deposition of particles (Itoh et al. 1985). In this region, the turbinate region, air is heated by blood supplied to the conchae and humidified by the mucous lining. The increased

surface area of the nasal cavity caused by the turbinates enhances the conditioning of the air (Marieb and Hoehn 2007). In this region the primary direction of flow is along the medial axis. Upon traversing the turbinate region the nasal septum and conchae end and the two cavities mix. This is known as the nasopharynx. Here the nasal cavity is relatively simple and the flow turns to flow down the body in the longitudinal axis towards the lungs. The nasopharynx comprises part of the pharynx which connects the nasal cavities to the oropharynx and the larynx.

For oral breathing, the aforementioned structures are not of concern as the inhaled air enters the body through the mouth and only interacts with the teeth and tongue in the oral cavity before turning down the body at the oropharynx. From this point inhaled air encounters the same structures whether breathing is nasal, oral, or a combination of both. From the oropharynx, flow is directed into the larynx through the laryngopharynx. The larynx controls access to the trachea and ensures solids and liquids from the mouth are directed to the esophagus using the epiglottis as a gate. Flow now enters the trachea, a structure of circular or elliptical cross-section which connects the extrathoracic airways and the lungs. Marieb and Hoehn (2007) provide an in-depth description of the nasal structures and further discussion of the functions these structures perform.

Deposition characteristics differ whether inhalation is via the oral or nasal pathway due to the different structures influencing the flow. Administration of therapeutic aerosols via the oral route has long been the preferred method as the oral airway filters less aerosol (Heyder et al. 1975). The aerosol deposition properties of the nasal passage remain relevant for atmospheric aerosols as humans of all ages tend to breathe nasally at rest (Bennett et al. 2008), and for pharmaceutical aerosols in cases where nasal delivery is necessitated. Such is the case for infants who are obligate nasal breathers and for young children who cannot learn the coordinated inhalation techniques associated with some oral inhalers. Recently some interest has shifted back to nasal delivery under the idea that short-acting agents could be delivered continuously during sleep (Zeman et al. 2017) or that patients already receiving noninvasive ventilation could be administered aerosol medications simultaneously with gas delivery (Walenga et al. 2014). Thus, quantification of nasal filtration properties in all ages is required for continued development of improved pharmaceutical aerosol devices and air quality standards.

Nasal deposition can be quantified through *in-vivo* techniques, *in-vitro* measurements in airway replicas, or *in-silico* simulations of fluid and particle dynamics in the airways; each method has its specific strengths and weaknesses. *In-vivo* measurements usually involve the inhalation of radiolabelled aerosol and subsequent nuclear imaging of the subject. This method not only provides

extrathoracic filtration but also regional distribution fractions all in one measurement; since breathing is performed naturally the time dependant properties of the respiratory system are also accounted for. Deposition as a function of particle size can only be measured by inhaling monodisperse aerosol and performing multiple measurements making this method costly and tedious in addition to the risks associated with radiation exposure inherent to this method. *In-vivo* nasal deposition measurements can also be performed by having participants hold their breath while aerosol is drawn through their nose and out their mouth. This method eliminates exposure to radiation however the flow path is non-natural and relies on significant patient cooperation. *In-silico* simulations eliminate radiation risks associated with nuclear *in-vivo* measurements and can provide extremely detailed regional deposition data in realistic inhalation scenarios. The geometries in which the simulations are performed must be acquired through nuclear imaging; however, these scans are normally done for other purposes. Due to the possibility of generating misleading results, simulations must be validated with either *in-vivo* or *in-vitro* measurements in identical geometries. *In-vitro* measurements in static airway replicas, while unable to account for time dependant airway morphology, address many of the issues associated with *in-vivo* measurements and serve as a starting point for *in-silico* simulations. Measuring deposition in airway replicas based on high resolution nuclear imaging of subjects scanned for reasons beyond the respiratory system eliminates additional radiation exposure to the patient, eliminates any need for patient cooperation, and allows deposition data to be obtained for any particle size under many varying flow conditions. *In-vivo*, *In-vitro*, and *in-silico* methods, and combinations thereof, have been used extensively to add to our understanding of extrathoracic deposition.

Adult nasal filtration has been studied extensively through all the above methods (Hsu and Chuang 2012; Walenga et al. 2014 and references therein) while relatively little has been studied pertaining to pediatric nasal deposition. *In-vivo* total deposition measurements have been reported of 20 children aged 5.5-15 years old (Becquemin et al. 1991) and 12 children 6-10 years old (Bennett et al. 2008) while *in-vitro* nasal filtration was measured in 14 replicas of the nasal airways of children aged 4-14 years old by Golshahi et al. (2011). As the focus shifts towards younger children the literature becomes sparser. Ultrafine aerosol deposition in three young children aged 1.5, 2.5, and 4 years was studied by Cheng et al. (1995) while inertial deposition was studied by Zhou et al. (2014) in two children aged 3 and 5 years and two infants aged 10 days and 7 months. Storey-Bishoff et al. (2008) focused on infant inertial filtration and measured deposition in nasal replicas of ten infants aged 3-18 months and the model of a 9-month old female published by Janssens et al. (2001). That study presented the first assessment of intersubject variability of

deposition in infants and a correlation which collapsed that variability onto a single curve. Golshahi et al. (2010) further studied the models created by Storey-Bishoff et al. by measuring the deposition of ultrafine aerosols in the ten airway replicas. The shape of those airways was studied by Javaheri et al. (2013) who identified an approximately average airway shape by combining 24 cross-sections from each geometry into 24 representative cross-sections and then reconstructing a three-dimensional airway. The resulting airway model, called an idealized geometry, has a structure similar to realistic airways yet is simplified. Idealized airway geometries are developed to be relatively simple to manufacture, compared to realistic airways, while mimicking the aerosol filtration properties of the population they are based on. These geometries, such as the 'Alberta Idealized Throat' model (Grgic et al. 2004), are invaluable tools aiding the design and development of pharmaceutical aerosol devices (Ciciliani et al. 2017; Sheth et al. 2017; Weers et al. 2015). Since extrathoracic deposition depends on the inhalation route and the size of the airway, and thus age of the patient, different idealized models for the nasal and oral airway of specific populations are required to mimic the deposition properties of the population under study. The 'Alberta Idealized Throat' (which has adult scale dimensions) was successfully scaled by Golshahi and Finlay (2012) to mimic oropharyngeal filtration of children aged 6-14 years old producing a geometry useful for experiments of aerosol delivery devices developed for pediatric use.

Very few infants younger than 3 months old have been studied in terms of nasal filtration. In addition to the 10 day old infant studied by Zhou et al. (2014), a 6 week old infant was studied by Swift (1991) and a premature infant of 32 weeks gestational age was studied by Minocchieri et al. (2008). The research presented in this thesis seeks to provide a more comprehensive understanding of the inertial filtration properties of neonatal and very young infants.

1.2 Objective

There are two primary objectives of this study: first, to quantify the deposition properties of neonatal and young infants aged 0-3 months and compare deposition in this population to that of older infants, and second, to investigate the ability of the infant idealized nose, or scales thereof, to mimic deposition in this younger population.

To achieve the first main goal new airway replica casts were constructed from computed tomography (CT) images of infants younger than 3 months old who underwent imaging for diagnostic reasons unrelated to the respiratory system. Measurement of inertial deposition in these models was carried out, the results of which were compared to deposition in 3-18 month old infants in multiple ways. Additionally, non-dimensional analysis of the deposition data was

performed to collapse the intersubject variability in the data onto a single curve resulting in a single equation describing deposition in the neonatal nasal replicas. Further, the expected average, and variance of, *in-vivo* total extrathoracic deposition was estimated.

The second objective was then investigated by producing multiple scaled models of the infant idealized nasal airway. The filtration properties of these geometrically similar models were measured under identical conditions in the same apparatus used to measure deposition in the nasal replicas. This allowed a straightforward comparison of aerosol filtration of the airway replicas to that of the scaled idealized models.

1.3 Thesis Structure

The following two chapters are manuscripts that have been submitted for publication. At the time of submitting this thesis they remain under review. Chapter 2 addresses the first major goal and details the development of neonatal nasal replicas, the physical characteristics of these models, and the experimental method followed to measure deposition in the models. The results are compared to deposition in 3-18 month old infants reported by Storey-Bishoff et al. (2008) and the ability of their predictive correlation to describe deposition in the newly developed models of younger infants is explored. Following this comparison, the suitability of the infant idealized model to mimic deposition in the neonatal population is explored in Chapter 3; the second major research goal of this project. Prospective scale factors to be applied to the full scale infant are developed. A suitable scale was identified by measuring deposition in three isotropically scaled models of the idealized infant nose and comparing to the deposition measurements of the nasal replicas. The ability to predict this scale factor based on airway characteristics and infant demographics was evaluated post hoc. The major results of this research are summarized in Chapter 4 and a brief look to future work is considered.

Chapter 2: Deposition of Micrometer-sized Aerosol Particles in Neonatal Nasal Airway Replicas

2.1 Introduction

Aerosolized medications are an indispensable tool for the treatment of respiratory ailments, allowing targeted delivery of therapeutic agents to the lungs and delivery of drugs with low oral bioavailability (Everard 2003). Conversely, aerosols in the form of airborne pollutants can be hazardous to health with effects ranging from mild irritation to cancer (Kampa and Castanas 2008). While the extrathoracic airways act to filter ambient particulate matter, particles making up therapeutic aerosols must successfully traverse these airways to achieve their desired effect in the lungs. In adults, the oral airway has long been known to filter less particulate matter than the nasal airway (Heyder et al. 1975) so has been preferred for the delivery of therapeutic aerosols. However, nasal delivery is relevant to populations such as infants, who are obligate nasal breathers, and young children who cannot learn to use an oral inhaler. Furthermore, since nasal breathing is common at rest at all ages (Bennett et al. 2008) lung exposure to atmospheric aerosols depends on nasal filtration. Therefore, the filtration properties of a target population's nasal airways must be well understood to aid in the design of effective pharmaceutical aerosolization devices and the development of air quality standards.

Deposition in adult nasal airways has been well investigated through *in vivo* and *in vitro* measurements and *in silico* simulations e.g. Hsu and Chuang (2012) and Walenga et al. (2014) and references therein. Far fewer studies have been carried out to quantify nasal deposition in children and have compared filtration in children to adults (Becquemin et al. 1991, Bennett et al. 2008, Golshahi et al. 2011, Phalen et al. 1989) but with varying results. Despite reports of increased infant mortality with exposure to increased levels of ambient particulate matter (Son et al. 2008, Woodruff et al. 1997), even fewer have studied the filtration properties of infant nasal airways. Storey-Bishoff et al. (2008) comprehensively measured nasal deposition in 11 different nasal models of infants aged 3-18 months old and identified a correlation describing the nasal filtration of these airways as a function of particle size, inhalation flow rate, and airway characteristic diameter. It is unclear if their correlation can be extrapolated to neonates or infants younger than 3 months old. Swift (1991) and Zhou et al. (2014) each present isolated *in vitro* measurements of nasal deposition in an infant younger than 3 months old but do not investigate enough subjects to account for the intersubject variability expected within this population. The filtration, and variability therein, of the nasal passage of neonatal infants remains to be fully described. We have

designed the present *in vitro* study to expand current understanding of neonatal nasal particulate filtration. This study presents the deposition characteristics of seven anatomically realistic nasal replicas of neonatal infants along with a correlation that provides average nasal filtration in this population. In addition, an estimate of the variability in deposition due to geometric dissimilarity, that is, variation in airway shape, in the population is provided.

2.2 Methods

2.2.1 Nasal Replica Models

Nasal replicas were constructed based on computed tomography (CT) scan data acquired under anonymity from the University of Alberta Diagnostic Imaging Archives with approval from the University of Alberta Research Ethics Office. Infants underwent imaging for health reasons unrelated to this study and in all cases the nasal airway was considered normal. The images were imported and segmented using Mimics software (Materialise, Leuven, Belgium). In-plane resolution of the scan images ranged from 260 to 434 μm and axial slice thicknesses ranged from 0.6 to 1.5 mm producing voxel sizes of 0.113 ± 0.063 mm^3. Airways were identified based on an upper density limit of about -240 Hounsfield units. Stereolithography files of the face and airway were smoothed in 3-Matic (Materialise) to eliminate roughness introduced by the discretization of the naturally smooth surfaces and then exported to the Magics software package (Materialise) where the model was created.

Each model consisted of three parts; the first part included the entire face and the airway just distal to the nasal valve, the second included the airway up to the nasopharynx and the final part extended from the nasopharynx through the larynx into the trachea. The outlet of the airway model was made such that it ended orthogonal to the axis of the trachea and the expected direction of flow. This multi-piece construction was used to accommodate removal of support material after rapid prototyping. The models were fastened together with machine screws and sealed externally with silicone sealant (737, Dow Corning, Midland, MI, USA). Models were printed with an Eden 350V (Stratasys, Eden Prairie, MN, USA) printer using VeroGray and VeroBlack photopolymer (Stratasys). The two materials have the same properties except colour and were used based on availability. The resolution of the build is 42 μm in the x- and y-axis (in plane resolution) and 16μm in z-axis (build direction). After printing and cleaning, the pieces were CT scanned to ensure support material had been adequately removed.

Select dimensions of the airways, including the airway volume and surface area, were obtained in the 3-Matic work environment for evaluation of dimensionless parameters. Storey-

Bishoff et al. (2008) found airway volume divided by surface area provided a length scale $D_{V/As}$ which collapsed intersubject variability, motivating consideration of these dimensions here. Additionally, Garcia et al. (2009) suggest a dimension, referred to herein as D_{Garcia}, based on nasal resistance which has also been found to fit inertial deposition data well by others (Golshahi et al. 2011; Zhou et al. 2014). Briefly, the procedure to measure this dimension involves taking pressure drop measurements across the nasal airway and obtaining the nasal resistance (R_{nose}) by fitting the resulting data to:

$$\Delta P = R_{nose} Q^{1.75} \tag{2.1}$$

where ΔP is the pressure drop across the model at corresponding flow rate, Q, through the model. The dimension is then obtained by evaluating

$$D_{Garcia} = \left(\frac{k\, L_{nose}}{R_{nose}}\right)^{4/19} \tag{2.2}$$

where L_{nose} is the length of the nose defined as the distance from the nostrils to the end of the septum and k is a constant depending on fluid properties (0.0181 kg/[($m^{10/4}$)·($sec^{1/4}$)] for air at standard conditions). The resulting dimension is the diameter of a circular pipe that has the same length and resistance as the nasal airway for turbulent internal air flow.

Pressure drop across the nasal airways was measured with a low range digital manometer (HHP-103; OMEGA Engineering, Stamford, CT, USA) at constant flow rates between 2 and 18 standard L/min. Least squares fitting was used to fit the pressure drop data as suggested by Garcia et al. (2009). The data fit this equation well with R^2 values greater than 0.99 for each subject. Demographic information and dimensions for each subject are given in Table 2.1.

Table 2.1: Subject demographics and airway characteristics

Subject	Age (days)	Sex	m (kg)	V (mm^3)	A_S (mm^2)	L_{nose} (mm)	R_{nose} ($Pa/(L/min)^{1.75}$)	$D_{V/As}$ (mm)	D_{Garcia} (mm)
1	5	F	3.50	4474	4229	31.15	6.489	1.06	2.42
2	9	M	3.57	4831	5190	39.64	16.46	0.93	2.10
3	9	F	3.54	4777	4767	34.22	3.094	1.00	2.89
4	34	M	N/A	4641	6817	44.16	18.28	0.68	2.10
5	52	F	6.30	4734	4967	42.83	18.78	0.95	2.07
7	78	M	6.60	5752	6855	43.12	17.09	0.84	2.12
8	79	M	5.80	8473	9621	46.42	2.725	0.88	3.17
Average	38	--	4.89	5383	6064	40.22	11.85	.906	2.41

m, body mass of infant at time of scan; V, volume of the nasal airway; A_S, surface area of the nasal airway; L_{nose}, length from the nostril to the end of the septum; R_{nose}, nasal resistance

2.2.2 Breathing Patterns

Deposition was measured under simulated tidal breathing conditions; a sinusoidal wave form was used. Breath parameters were selected based on values observed in the literature and such that physiologically realistic inhalation flow rates would be achieved. Haddad et al. (1979) found that the duty cycle does not change significantly with age in the first four months of life. Thus, a duty cycle of 0.32 was selected based on the mean observed value. A realistic range of average inhalation flow rates were identified based on minute ventilation data including a minimum of 1.6 L/min based on 10th centile minute ventilation of 142.9 mL/(min·kg) for an infant with mass 3.5 kg and a maximum of 14.6 L/min based on 90th centile minute ventilation of 707.7 mL/(min·kg) and an infant with a mass of 6.6 kg (Estol et al. 1988). It should be noted that a 6.6 kg infant is out of the range studied by Estol et al. (1988) however this only represents a 19% increase from a maximum based on 613 mL/(min·kg) minute ventilation and a 6.4 kg infant (giving 12.3 L/min) which are values observed by Fuchs et al. (2011) for unsedated infants during quite sleep. Respiratory rates in the range of 40 to 60 breaths per minute are common (Rusconi and Castagneto 1994) and values as extreme as 20.7 and 117.5 breaths per minute have been reported (Richards et al. 1984). Estol et al. (1988) give 10th and 90th centiles for body mass normalized tidal volume as 2.21 and 10.34 mL/kg and Fuchs et al. (2011) observed a maximum of 11.8 mL/kg giving a tidal volume range of 7.7 mL to 77.9 mL. After identifying acceptable ranges for each breath defining parameter, seven different breath profiles were selected. In the present work, the tidal volume range was extended up to 100 mL for comparison with deposition in infants reported by Storey-Bishoff et al. (2008). The defining parameters are listed in Table 2.2.

Table 2.2: Breath defining parameters

f (min^{-1})	V_t (mL)	Q (L/min)
30	19	1.78
50	21	3.28
89	17	4.73
50	45	7.03
75	40	9.38
55	68	11.69
45	100	14.06

f, respiratory rate; V_t, tidal volume;
Q, average inhalation flowrate = $(1/0.32)\cdot V_t \cdot f$

2.2.3 Experimental Apparatus

Deposition measurements were carried out in an aerosol exposure plenum built to the specifications presented by Golshahi et al. (2011). In brief, the plenum is cubic with side length of 0.6 m; the top section is a mixing region 10 cm tall where two opposing fans create a well-mixed aerosol which is introduced to the exposure region (45 cm tall). The two regions are separated by a flow straightener to minimize secondary flow patterns in the supply air. The flow straightener is a 2 inch (5 cm) thick aluminum honeycomb with 0.25 inch hexagonal cells (HoneyCommCore, Jupiter, FL, USA).

A rigid piping system of 3/8" NPT stainless steel pipe and 3/4" (.0675" wall) aluminum tubing carried the sampled aerosol to an electrical low pressure impactor (ELPI) (Dekati Ltd., Kangasala, Finland) for classification. Aerosol of jojoba oil (ρ = 870 kg/m^3) was generated using a 1-jet Collison nebulizer (MesaLabs, Butler, NJ, USA) operated at approximately 5 psi connected to the building compressed air source; the resulting aerosol had a mass median aerodynamic diameter of 2.4 μm and a geometric standard deviation of approximately 2 (estimated by interpolating the discrete cumulative distribution measured by the ELPI).

The ELPI draws a constant flow of 30 L/min; this flow was matched by flow control on a tank of extra dry compressed air (Praxair, Danbury, CT, USA) such that there was no flow through the model while the ELPI was operating. This flow rate was monitored with a mass flowmeter (4043, TSI Inc., Shoreview, MN, USA) throughout the experiments. Flow profiles were created by an ASL 5000 Breathing Simulator (IngMar Medical, Pittsburgh, PA, USA). As was done by Storey-Bishoff et al. (2008), to eliminate the issue of large dead space in the experimental apparatus, the exhale portion of the breath was directed through a check valve near the ASL 5000; in this way the

airway replicas were tested under inhalation only and were stagnant during the exhalation phase of the breath. Flow profiles were recorded with another TSI 4043 flowmeter at a 10 ms sampling rate.

Two sampling lines extended into the aerosol plenum, one a blank line for characterizing the aerosol within the plenum, the other the model line which aerosol first traversed an airway replica before being routed to the ELPI. Rigid piping was used to eliminate any differences in particle deposition occurring within the two sampling lines; identical fittings and lengths were used in each line. Aerosol flow was switched between the two lines and directed to the ELPI with a three way, quarter turn ball valve. A schematic of the deposition measurement system is shown in Figure 2.1.

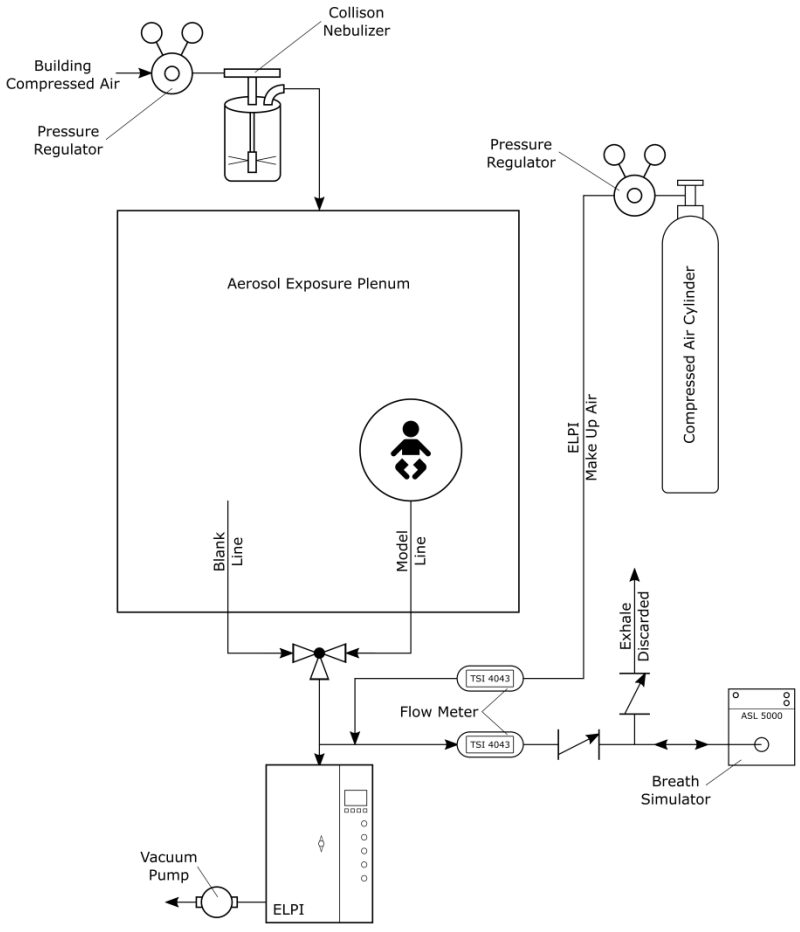

Figure 2.1: Schematic of experimental apparatus

2.2.4 Experimental Design

Each measurement consisted of two minutes of sampling through the blank line, two minutes through the model line, and another two minutes through the blank line. Sampling through the blank line twice was done to ensure aerosol concentrations were constant for the duration of

the measurement. Deposition was measured by comparing the aerosol sampled through the blank line to that sampled through the model line on a bin-by-bin basis. The ELPI provides concentration data for 12 particle size bins with aerodynamic diameter centres between 45 nm and 9 μm. Only data for the range of particles dominated by inertial deposition was analyzed. The largest bin had too few counts to provide meaningful data. Data for bins with geometric centres of 0.53, 0.83, 1.34, 2.12, 3.34 and 5.54 μm were thus used. The fraction of particles depositing in the model is given by:

$$\eta = \frac{c_{blank} - c_{model}}{c_{blank}} \tag{2.3}$$

Here, c_{blank} is the average concentration measured during both periods of sampling through the blank line (representative of the aerosol entering the model) and c_{model} is the average concentration measured after passing through a nasal replica. Note that due to added resistance in the model line, a slightly smaller tidal volume is generated by the ASL 5000 and thus the concentration measured must be corrected for the reduced number of particles entering the model simply due to a smaller volume of aerosol entering. This correction is achieved by multiplying c_{model} by the ratio of tidal volume measured through the blank line to the tidal volume measured through the model. The correction factor was calculated for each subject and each breathing pattern independently.

To ensure the validity of deposition measurements, several validations were made prior to carrying out the experiment. Sampling through two blank lines of identical length showed no difference in aerosol concentration which verifies that deposition within the piping was equal in each branch and thus not skewing deposition measurements systematically higher or lower. Sampling through blank lines of different lengths and/or different orientations allowed the spatial dependence of the aerosol distribution to be checked. It was found that the aerosol distribution within the exposure plenum did not depend on spatial coordinate as equal concentrations were measured through both sampling lines when sampling at different points within the chamber. This justifies the assumption that the aerosol concentration measured by the sampling line is indicative of the concentration entering the nostrils of the nasal replicas. Finally, deposition measurements were performed in the two youngest nasal replicas made by Storey-Bishoff et al. (2008) using the breath profiles reported in that study. Good agreement between the new measurements and the reported values provided further confidence in the experimental apparatus.

Deposition was measured in each nasal replica for each breath profile; each measurement was repeated three times. The standard deviation of repeated deposition measurements was on average 0.45 % indicating repeatability was good. Statistical analysis and numerical methods were

performed in MATLAB (R2014a, MathWorks, Natick, MA, USA), a significance level of α = 0.05 was used for statistical analysis. The Levenberg-Marquardt algorithm with unit weighting was used for non-linear least squares fitting.

2.3 Results and Discussion

Although it is expected there will be large spread in the data points when plotted against the well-known impaction parameter, it provides a starting point for comparison of the deposition measured in the neonatal models to that of the infant models. Figure 2.2 uses the impaction parameter to compare deposition in the younger neonate models and the older infant models studied by Storey-Bishoff et al. (2008) and additionally to the deposition measured in a nasal replica of a 10 day old infant under constant flow reported by Zhou et al. (2014).

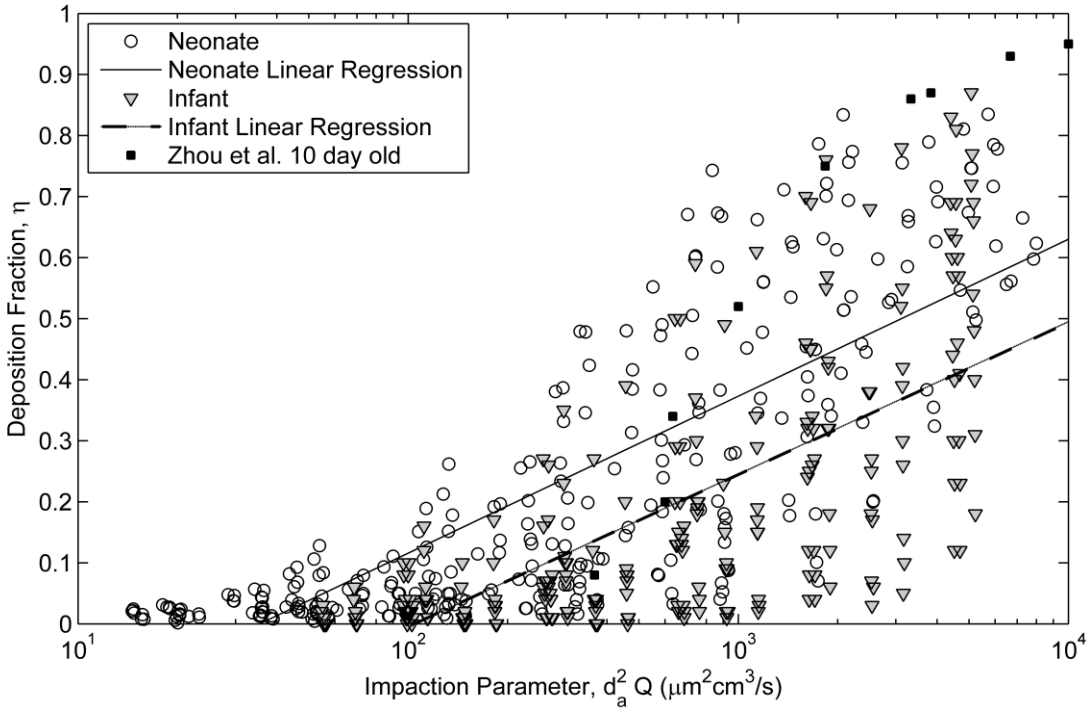

Figure 2.2: Comparison of deposition in population of neonate models (this study) to deposition in the population of infant nasal airways (Storey-Bishoff et al. 2008) and to deposition in a 10 day old infant (Zhou et al. 2014).

While there is substantial overlap in the data sets due to intersubject variability, significantly more deposition is measured in the neonatal population than the infant population for a given impaction parameter (p<0.001, t-test against regression coefficients). The slopes of the neonate and infant linear regressions are not statistically different, but for any given impaction parameter there is an average of about 12 % (absolute) more deposition in a neonate versus an infant.

Agreement is seen in the deposition measured by Zhou et al. (2014) and the neonatal population studied here although it appears that there may be higher deposition measured compared to our neonate models at the higher impaction parameter range. This could be due to roughness associated with construction of their model; Zhou et al. (2014) used rapid prototyping with a layer thickness of approximately 0.25 mm, whereas our models were built with a layer thickness of 16 μm. Kelly et al. (2004) and Schroeter et al. (2011) have shown that excessive surface roughness of the nasal model can affect deposition, exhibiting higher deposition that asymptotes with decreasing roughness to that measured in a smooth model. For this reason neither the Zhou et al. (2014) nor Swift (1991) data (3 mm surface roughness) will be considered further here. With a layer thickness that is 3 times thinner than the smoothest models tested by Kelly et al. (2004), we believe that wall roughness effects are negligible in our models.

The impaction parameter does not include any subject specific factor and thus shows how significant the variation in deposition can be within a population. This is evident in Figure 2.3 which compares the deposition between each neonate subject as a function of the impaction parameter.

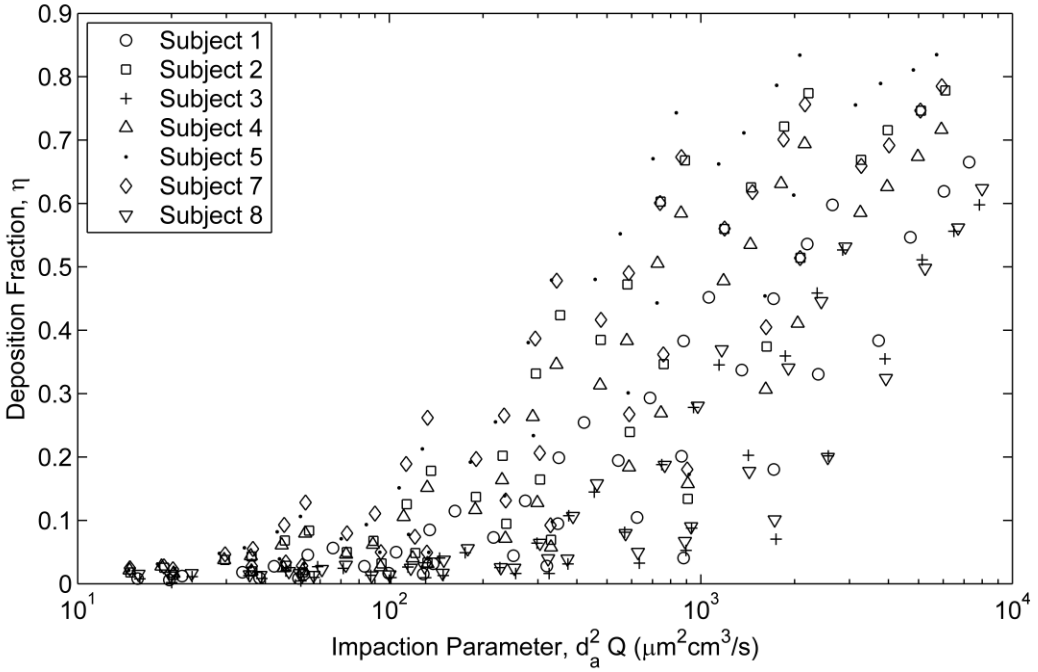

Figure 2.3: Deposition for each neonate nasal model as a function of impaction parameter

The inclusion of subject specific factors to account for intersubject variability is desirable to provide a better estimate of the average deposition in the population. Hounam et al. (1971) first identified transnasal pressure drop as one such factor and modified the impaction parameter by

replacing flow rate with the resulting pressure drop. Plotting deposition against this pressure-drop-based impaction parameter (Figure 2.4) reduces the scatter of the data considerably.

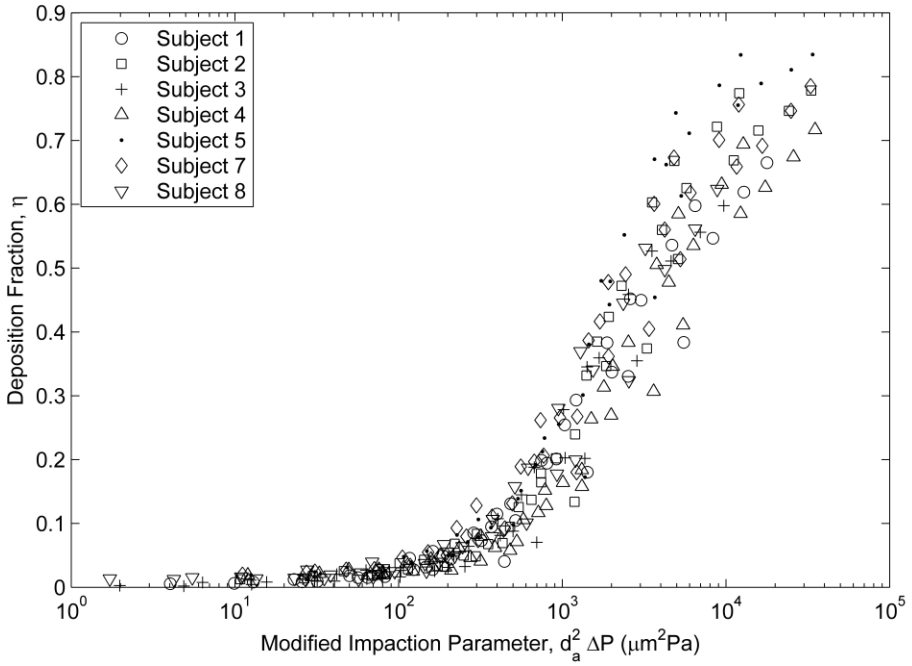

Figure 2.4: Deposition as a function of pressure-drop-based impaction parameter

This parameter does not explicitly include any characteristic length scale, which particle dynamics suggest should be included in the form of the particle Stokes number, but the pressure drop across a duct is known to be strongly correlated with duct diameter. This pressure based impaction parameter was further varied by Garcia et al. (2009) who found adult nasal deposition data was better collapsed by a parameter of $d_a^2 \Delta P^{2/3}$; however, use of this parameter did not improve the description of our neonatal nasal deposition data compared to the use of $d_a^2 \Delta P$.

2.3.1 Non-Dimensional Analysis

Following previous work (Cheng 2003; Golshahi et al. 2011; Storey-Bishoff et al. 2008; Zhou et al. 2014), further non-dimensional analysis of the deposition data should allow extension of these deposition results to other carrier gases, larger particle sizes, and other sizes of similarly shaped geometries. Using deposition results in this way is subject to the non-dimensional parameters remaining within the range studied and that impaction remains the dominating mechanism of deposition. Extension to non-similar geometries is a violation of scaling laws (Çengel and Cimbala 2010) (different subjects are not exact scales of one another) and Storey-Bishoff et al. (2008) attribute the discrepancies in measured deposition and their non-dimensional equation to this fact. Nevertheless, it is interesting to explore the ability of the correlation developed by Storey-

Bishoff et al. (2008) for the nasal filtration in 3-18 month old infants to describe deposition measured in the neonatal models. With a trivial modification to account for our use of the standard definitions of Reynolds number (*Re*) and Stokes number (*Stk*) the correlation of Storey-Bishoff et al. is:

$$\eta = 1 - \left(\frac{3.660 \cdot 10^5}{3.660 \cdot 10^5 + Stk^{1.057} Re^{1.118} \left(D_{V/A_S} / D_{avg} \right)^{-2.840}} \right)^{0.8510} \tag{2.4}$$

where D_{avg} is the average volume over surface area diameter reported by Storey-Bishoff et al. 2008 as 1.20 mm. The definitions of *Stk* and *Re* are

$$Stk = \frac{2Q\rho_0 d_a^2 C_c}{9\pi\mu_f D^3} \tag{2.5}$$

$$Re = \frac{4Q\rho_f}{\pi\mu_f D} \tag{2.6}$$

where Q is the average flow rate during the inhalation period of the breath, ρ_0 is the reference density (1000 kg/m^3), d_a is the particle aerodynamic diameter, μ_f is the fluid dynamic viscosity (1.8x10^{-5} kg/m·s for air), D is the characteristic diameter of the geometry, ρ_f is the fluid density (1.10 kg/m^3 for air at 93 kPa, normal ambient pressure at the location of the experiment), and C_c is the Cunningham correction factor that accounts for non-continuum effects given by

$$C_c = 1 + \frac{\lambda}{d_a}\left[2.34 + 1.05 \exp\left(-0.37 \frac{d_a}{\lambda}\right)\right] \tag{2.7}$$

where λ is the mean free path of air (74 nm for air at 21°C and 93 kPa). Using these definitions, measured deposition can be plotted with an abscissa of the combination of dimensionless parameters from Equation 2.4 as is done in Figure 2.5.

While this deposition parameter does not collapse the intersubject variability in this population, the correlation does a fair job predicting the average deposition. Recently, Yang et al. (2017) examined the ability of several correlations to predict oral extrathoracic aerosol deposition in adults by comparing to *in-vivo* measurements. They found that while correlations can predict average deposition in a population, they fail to accurately predict subject specific deposition. This failure was attributed to extrapolation of the predictive correlations to conditions they were not developed under such as different average inhalation flow rates, tidal volumes, and respiratory rates. Errors were also attributed to the violation of geometric similarity in the use of dimensional analysis. These sources of error are present in this study when attempting to use the correlation developed by Storey-Bishoff et al. (2008) to collapse deposition data in smaller models of different subjects tested under different breathing conditions.

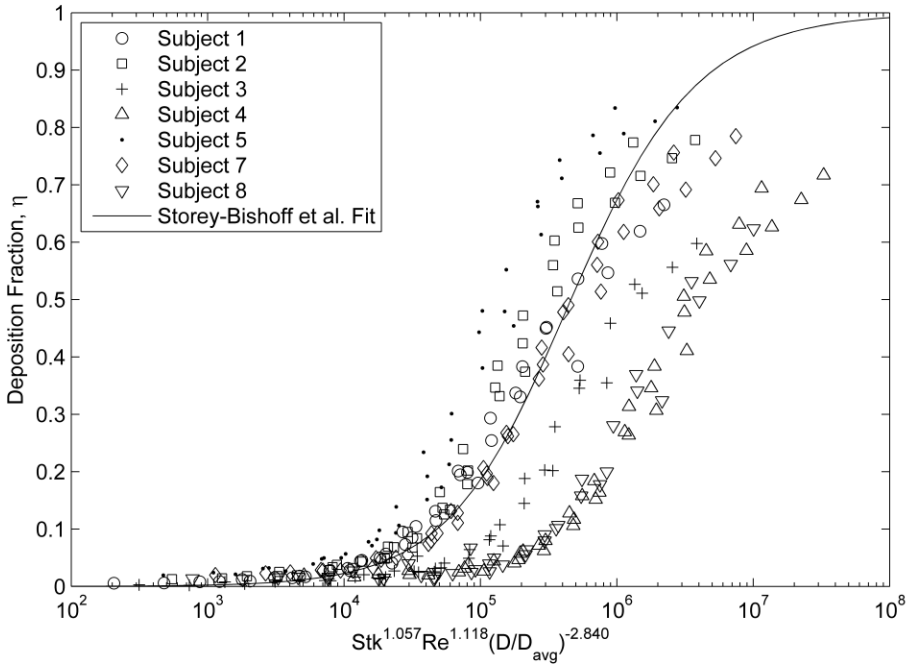

Figure 2.5: Deposition measured in neonatal nasal airways compared to the correlation developed by Storey-Bishoff et al. (2008) for deposition measured in infants (r^2 = 0.47)

To further collapse intersubject variability in the presentation of the data, other combinations of the dimensionless parameters evaluated using the different characteristic diameters were explored. The Euler number (Eu), a dimensionless pressure drop, was also explored based on the results of plotting deposition vs. the pressure based impaction parameter (Figure 2.4) and is defined as:

$$Eu = \frac{\Delta P}{\rho_f U^2} = \frac{\Delta P \pi^2 D^4}{16 \rho_f Q^2} \tag{2.8}$$

where ΔP is the transnasal pressure drop at corresponding average inhalation flow rate, Q. Different products of dimensionless parameters (always including the Stokes number since aerosol theory describes the value of the Stokes number as being the extent to which a particle's path deviates from streamlines and thus may undergo inertial deposition) were used as the abscissa; the powers of each parameter were allowed to vary and found through non-linear least squares regression. The highest coefficient of determination value, r^2, found for each deposition parameter evaluated with each characteristic diameter is listed in Table 2.3.

Table 2.3: Summary of r^2 values for each characteristic diameter. Values of α, β, γ are different in each case found using non-linear least squares fitting

Deposition Parameter	$D = D_{V/As}$	$D = D_{Garcia}$
Stk^{α}	0.69	0.84
$Stk^{\alpha}Re^{\beta}$	0.76	0.94
$Stk^{\alpha}Eu^{\beta}$	0.81	0.84
$Stk^{\alpha}Re^{\beta}(D/D_{avg})^{\gamma}$	0.78	0.96
$Stk^{\alpha}Re^{\beta}Eu^{\gamma}$	0.97	0.97
$Stk^{\alpha}Eu^{\beta}(D/D_{avg})^{\gamma}$	0.82	0.89

While optimizing the constants of Equation 2.4 improved the r^2 value for the neonate data, this characteristic diameter ($D_{V/As}$) and deposition parameter combination (Re, Stk, and D/D_{avg}) does not fully collapse the data, contrary to observations by Storey-Bishoff et al. (2008). Interestingly, the collapse is essentially the same for the two characteristic diameters studied when the Euler number is used despite fits excluding Eu being better when using D_{Garcia}. This is likely due to the inherent inclusion of the transnasal pressure drop in this characteristic diameter via the nasal resistance factor in the calculation. Since pressure drop is not only sensitive to the size of the airway, but also to the shape, inclusion of this measurement can be thought of as including information about some of the geometric dissimilarities between models. For example, a large but convoluted airway may have similar filtration properties as a smaller, simpler airway which would not be immediately clear based on purely geometric measurements such as $D_{V/As}$, whereas comparing the nasal resistance provides some insight to the shape of the airway. That is to say, $D_{V/As}$ is purely a measure of airway size, while D_{Garcia} includes not only the airway size but also some degree of measure of its shape. Further, including the Euler number in the deposition parameter introduces this measure of shape to the correlation when evaluating with $D_{V/As}$. Since the shape cannot be fully defined with only these two measures, the remaining dissimilarity remains in the data, to the same extent, regardless of choice of characteristic diameter.

Here, the Euler number is found to significantly improve the fit, in contrast to the observation by Golshahi et al. (2011) in older children. The best correlation found is

$$\eta = 1 - \left(\frac{14590}{14590 + Stk^{1.2201}Re^{1.7742}Eu^{1.5772}}\right)^{0.3687} \tag{2.9}$$

where $D_{V/As}$ is used in the evaluation. Figure 2.6 demonstrates the ability of this deposition parameter and resulting correlation to describe the deposition in these models.

The rate at which infants develop in the first years of life may account for the fact that inclusion of the Euler number was not required to fit deposition in children (Golshahi et al. 2011) as

intersubject variability due to the degree of development of the nasal passage, and thus shape, may be less in that population. This is corroborated by the observations of Golshahi et al. (2011) who found that infant nasal deposition was higher than in children, with considerable scatter remaining in the data when applying the infant nasal deposition equation to child deposition data, and that a single correlation to describe deposition in infants and children could not be developed. They also note that nasal deposition in children and adults as a function of impaction parameter showed considerable overlap, while for a given impaction parameter deposition for infants is generally higher. This is attributed to the similar magnitude of child and adult characteristic diameters opposed to much smaller diameters of infants.

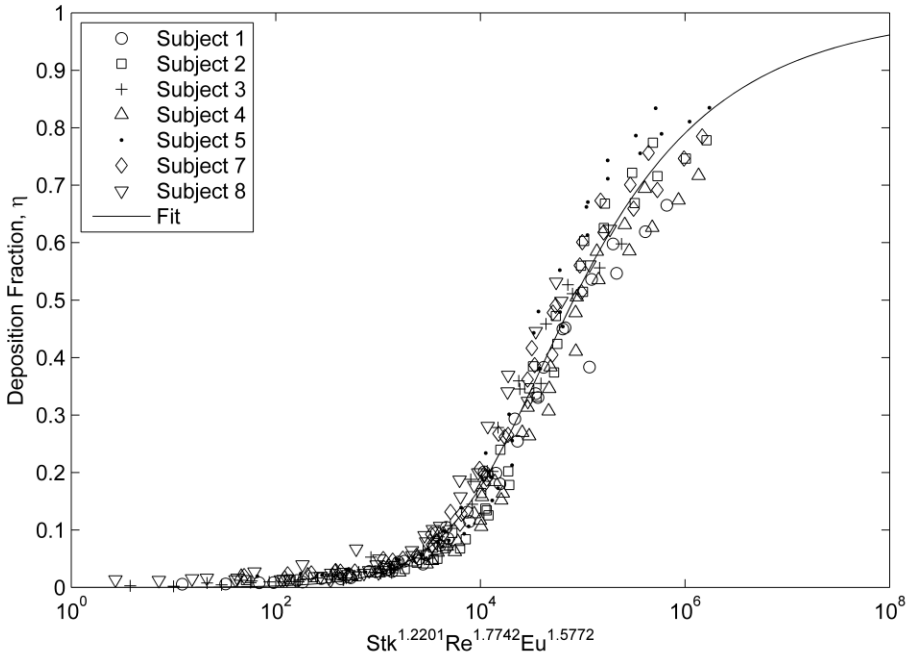

Figure 2.6: Deposition in neonatal nasal airways vs. non-dimensional deposition parameter, characteristic diameter defined D=V/A_S, fit defined in Equation 2.9, r^2 = 0.97

Equation 2.9 can be evaluated with population average values to represent the average deposition expected in the neonatal subjects studied here. Using the average $D_{V/As}$ = 0.906 mm, an inhalation flow rate of 4.3 L/min and thus a pressure drop of 152 Pa (obtained using the average nasal resistance), a 2 μm particle has a 14.1 % deposition fraction. Storey-Bishoff et al. (2008) report a filtration of only 2.0 % for the same particle diameter and flow rate for their population average $D_{V/As}$ = 1.20 mm, further exhibiting the increased deposition measured in the younger population.

2.3.2 Estimating Total In-Vivo Deposition Variability

While the result of non-dimensional analysis on the *in-vitro* data shows a strong ability to account for intersubject variability and may suggest the potential for Equation 2.9 to be used in a predictive capacity, the accuracy of predictive correlations on a subject specific basis has recently been called into question. Alternatively, these equations have been found to well predict the average deposition of a population (Yang et al. 2017). The errors associated with using deposition correlations in a predictive capacity were further analyzed by Ruzycki et al. (2017) who proposed a novel approach using the deposition equation to provide an estimate of the variance of deposition expected in a population. Their predictions accurately mirrored the *in-vivo* results of Yang et al. (2017) and thus present an approach for a deposition correlation to be used to predict an average and standard deviation of *in-vivo* deposition in a population, as opposed to expected values in individual subjects.

The details of this analysis are described by Ruzycki et al. (2017), so will not be fully described here. In summary, the total deposited fraction on a mass basis is calculated by integrating the deposition of particles over a defined aerosol distribution. The average deposition is calculated using population average values for inhalation flow rate and characteristic diameter. Then, using a method based on the concept of propagation of uncertainty, an estimate for the variance in total deposition is obtained by combining the variance in deposition caused by the variance of each constitutive parameter using the root-sum-of-squares.

To use this method, the variance of each parameter must be known and thus data for each parameter must follow a known distribution. The nasal resistance data fails the Anderson-Darling normality test (p = 0.04 using adtest function in MATLAB) and thus the variance in deposition due to nasal resistance cannot be identified and the method cannot be performed using Equation 2.9. A simplified equation which does not depend on transnasal pressure drop is required for this method. Deposition as a function of only the Stokes number in our subjects is given by

$$\eta = 1 - \left(\frac{9.7}{9.7 + Stk^{0.9757}}\right)^{0.9251} \tag{2.10}$$

where Stk is evaluated with $D_{V/As}$. The simplicity of this equation reduces its accuracy but permits the estimation of deposition variance. The fit of this deposition correlation is shown in Figure 2.7.

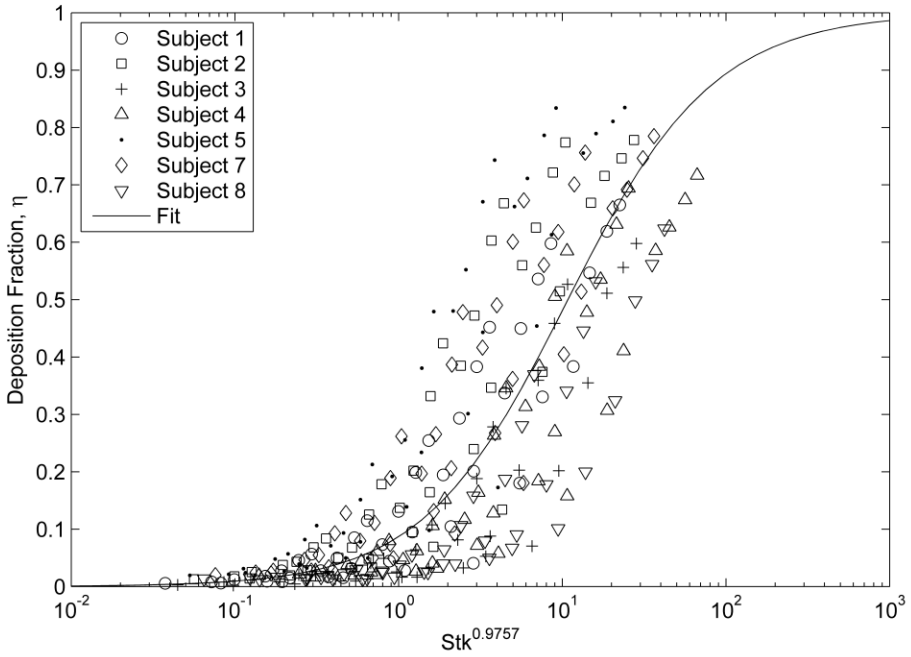

Figure 2.7: Neonatal nasal deposition as a function of Stokes number, characteristic diameter defined D=V/A$_S$, fit defined in Equation 2.10, r^2 = 0.69

Using this simplified equation allows direct application of the method as developed by Ruzycki et al. (2017) where variation in deposition, s_η, is due to variation in flow rate, s_{η_Q}; characteristic diameter, s_{η_D}; and geometric dissimilarity, $s_{\eta_{gd}}$. The exclusion of the Euler number in the deposition parameter can be thought of as returning shape differences to the data, these differences being then accounted for by the variance in deposition due to geometric dissimilarity.

The distribution of input parameter values is required to evaluate s_{η_Q} and s_{η_D}. The characteristic dimensions of our nasal models are known and pass the Anderson-Darling normality test ($p > 0.05$) so the average and standard deviation of this sample (D = 0.906 ± 0.123 mm) can be used. An expected distribution of inhalation flow rates for these subjects is also required. Haddad et al. (1979) report average inhalation flow rate during quiet sleep throughout the first four months of life; their reported results for birth to three months of age have been pooled to give an estimate of the expected distribution of flow rates of 2.90 ± 1.04 L/min.

Examining the result of individually varying each parameter to values one standard deviation above and below the average value (Table 2.4) leads to estimates of the variability due to flow rate and characteristic diameter. For example, variation due to inhalation flow rate is found by calculating deposition at a flow rate one standard deviation below the average (Q_1) and one

standard deviation above the average (Q_2) yielding values for η_{Q1} and η_{Q2} respectively. Note that total deposition is calculated by integrating deposition across the aerosol distribution as was done by Ruzycki et al. (2017). This requires a specified aerosol distribution; an MMAD of 3.7 μm and GSD of 2 were used for illustrative purposes to define the aerosol here, which are the values used by Ruzycki et al. (2017). The magnitude of the difference in calculated deposition is two times the variation due to flow rate (i.e. $2\ s_{\eta_Q} = |\eta_{Q2} - \eta_{Q1}|$) since flow rate has been varied plus and minus one standard deviation from the mean. The same procedure is followed for variation due to characteristic diameter. The resulting estimate of variation in deposition due to flow rate is $s_{\eta_Q} =$ 5.7 %, and variation in deposition due to characteristic diameter is $s_{\eta_D} = 6.4$ %.

Table 2.4: Total deposition (on a mass basis) of aerosol with MMAD of 3.7 μm and GSD of 2

	Flow Rate, Q, (L/min)	Characteristic Diameter, $D_{V/As}$, (mm)	Deposition, η, (%)
Average	$Q_{avg} = 2.90$	$D_{avg} = 0.906$	$\eta_{avg} = 29.8$
Variation due to Flow Rate	$Q_1 = Q_{avg} - s_Q = 1.86$	$D_{avg} = 0.906$	$\eta_{Q1} = 23.3$
	$Q_2 = Q_{avg} + s_Q = 3.94$	$D_{avg} = 0.906$	$\eta_{Q2} = 34.7$
Variation due to Characteristic Diameter	$Q_{avg} = 2.90$	$D_1 = D_{avg} - s_D = 0.783$	$\eta_{D1} = 36.9$
	$Q_{avg} = 2.90$	$D_2 = D_{avg} + s_D = 1.029$	$\eta_{D2} = 24.2$

The estimate for variation due to geometric dissimilarity is obtained by examining the errors associated with using Equation 2.10 to describe deposition in the nasal replicas. If the characteristic diameter fully defined the shape of the airway, the data points would fall on a single curve (which is the intent of non-dimensional analysis). Since the characteristic diameter of the nasal replicas and inhalation flow rates during deposition testing are well quantified, presumably the residuals associated with the non-dimensional correlation are due to shape differences in the nasal replicas not captured by the characteristic diameter, that is, geometric dissimilarity. Plotting the deposition prediction obtained using Equation 2.10 versus the measured *in-vitro* deposition allows these errors to be inspected (Figure 2.8). Using the fact that 95% of the data lie within 2 standard deviations of the mean leads to an estimate of the variation due to geometric dissimilarity. In this case, 95% of the data are bounded by linear bands 32% above and below the line of identity (where the model perfectly describes the *in-vitro* data) yielding a variation due to geometric dissimilarity of $s_{\eta_{gd}} = 16$ %.

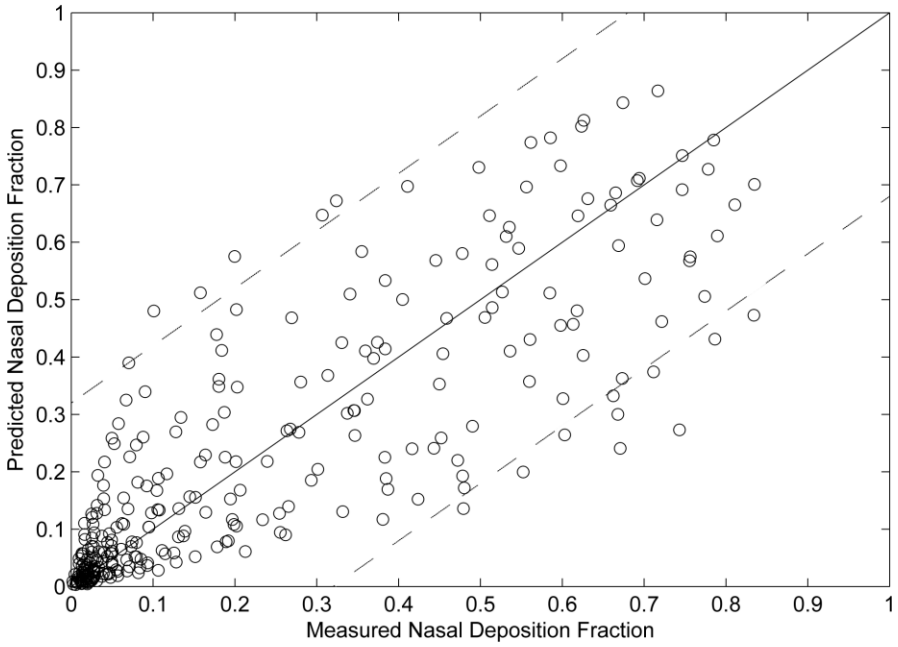

Figure 2.8: Predicted deposition (using Equation 2.10) versus *in-vitro* measured deposition. Solid line indicates line of identity; dashed lines bound 95% of the data.

The estimates of the three identified sources of variation yield a first-order estimate of the total variation in nasal deposition through the application of the ℓ^2-norm:

$$s_\eta = \sqrt{s_{\eta_Q}^2 + s_{\eta_D}^2 + s_{\eta_{gd}}^2} \tag{2.11}$$

Evaluating Equation 2.11 gives a standard deviation of $s_\eta = 18.1$ %. Thus, for the population of infants aged zero to three months, breathing nasally, during sleep, and receiving an aerosol with an MMAD of 3.7 μm and GSD of 2, one can expect 29.8 ± 18.1 % of the inhaled aerosol to deposit in the nasal passage. Repeating the above calculations using instead MMADs of 2.7 and 4.7 μm with the same conditions and a constant GSD of 2, we find average and standard deviations of deposition of 21.1 ± 17.5 % and 37.2 ± 18.6 %, respectively. Similar analysis can be performed for other aerosol distributions and inhalation flowrates to provide average nasal deposition and expected variance for the given conditions.

Although this method was developed based on a combination of *in-vivo* and *in-vitro* measurements and for oral inhalation in adults, the underlying method is valid. Estimates obtained in this way are thus the best currently available estimates of nasal deposition and expected variance in a population of neonatal infants. Comparison to *in-vivo* measurements to validate these

estimates is desirable. However, due to the risks associated with making these measurements using current technology (radiation exposure to a developing infant) and the degree of cooperation which would be required of the infants, this remains a topic for future research.

Comparing these results to those reported by Ruzycki et al. (2017) for oral, tidal breathing in adults is of some interest (Table 2.5). As expected, total deposition is much higher in the neonatal population despite the significantly lower inhalation flow rates. This is due to the route of inhalation and the size of the airways. It has long been known that, for adults, oral delivery of aerosols is favourable over nasal delivery since the nasal airway filters particles more effectively than the oral airway (Heyder et al. 1975). Coincidentally, the variations due to flow rate and due to characteristic diameter are comparable between the two cases. Thus, the increased variation in deposition in neonates is primarily due to increased variation due to geometric dissimilarity; in adults this variation is only 5%. This major difference in the two models is likely due to the inhalation route and the previously mentioned rate at which infants develop. Storey-Bishoff et al. (2008) compared the collapse of deposition data in oral and nasal geometries and attributed the additional dependence on characteristic diameter to describe infant nasal deposition partly to the increased extent that the nasal cross-sectional area departs from a circular shape. The same observation is made here where transnasal pressure drop (additional information about the airway shape) was required to fully collapse the deposition data in neonates. The oral cross-sectional area is much more circular and thus a given characteristic diameter better defines the oral airway reducing variation due to geometric dissimilarity. Further, geometric dissimilarity in the population of neonatal infants is likely higher due to the developing nature of infants. Since the airways of neonatal infants are growing and developing it is expected there would be larger shape variations within the population when compared to the fully developed oral airways of adults. Finally, in a relative sense, the variability in deposition is not vastly different between populations. The expected variation in neonatal nasal deposition is 60% of the average value whereas the variation in adults is 53% of the average.

Table 2.5: Comparison of average and variability in total deposition in adults (Ruzycki et al. 2017) and neonatal infants (*in-vitro*) when normally inhaling an aerosol with MMAD 3.7 μm and GSD of 2

	Neonates	Adults
Deposition, η (%)	30 ± 18	19 ± 10
Route of Inhalation	Nasal	Oral
Inhalation flowrate, Q (L/min)	2.90 ± 1.04	19.1 ± 5.6
s_{η_Q} (%)	5.7	4.1
s_{η_D} (%)	6.4	7.7
$s_{\eta_{gd}}$ (%)	16	5.0

2.4 Conclusions

Inertial nasal filtration in infants between the ages of 5 and 79 days has been quantified via *in-vitro* measurements. Increased deposition was measured in this population compared to existing *in-vitro* data (Storey-Bishoff et al. 2008) in infants aged 3 to 18 months. An empirical equation describing the deposition in our neonatal models was identified, with the best fit obtained by including non-dimensional pressure drop in the form of the Euler number in addition to the Stokes and Reynolds numbers. A simplified equation depending only on Stokes number was also identified; using this Stokes-number-only equation an estimate of the variance in nasal filtration expected within the population of neonatal infants is provided. Using this method, the Stokes-number-only equation can be used to predict an expected intersubject variation of total nasal aerosol deposition within a neonatal population. This work may be helpful to those designing aerosol treatments for infant respiratory ailments and to those studying the risks associated with the exposure of infants to ambient particulate matter.

2.5 Works Cited

Becquemin M.H., Swift D.L., Bouchikhi A., Roy M., Teillac A. (1991). Particle Deposition and Resistance in the Noses of Adults and Children. The European Respiratory Journal, 4(6):694-702.

Bennett W.D., Zeman K.L., Jarabek A.M. (2008). Nasal Contribution to Breathing and Fine Particle Deposition in Children versus Adults. Journal of Toxicology & Environmental Health, 71(3):227-237.

Çengel Y.A., Cimbala J.M. (2010). Fluid mechanics: Fundamentals and Applications. McGraw-Hill Higher Education, Boston.

Cheng Y.S. (2003). Aerosol Deposition in the Extrathoracic Region. Aerosol Science & Technology, 37(8):659.

Estol P., Priz H., Pintos L., Nieto F., Simini F. (1988). Assessment of Pulmonary Dynamics in Normal Newborns: A Pneumotachographic Method. Journal of Perinatal Medicine, 16(3):183-192.

Everard M.L. (2003). Inhalation Therapy for Infants. Advanced Drug Delivery Reviews, 55(7):869-878.

Fuchs O., Latzin P., Thamrin C., Stern G., Frischknecht P., Singer F., Kieninger E., Proietti E., Riedel T., Frey U. (2011). Normative Data for Lung Function and Exhaled Nitric Oxide in Unsedated Healthy Infants. The European Respiratory Journal, 37(5):1208-1216.

Garcia G.J., Tewksbury E.W., Wong B.A., Kimbell J.S. (2009). Interindividual Variability in Nasal Filtration as a Function of Nasal Cavity Geometry. Journal of Aerosol Medicine and Pulmonary Drug Delivery, 22(2):139-155.

Golshahi L., Noga M.L., Thompson R.B., Finlay W.H. (2011). In Vitro Deposition Measurement of Inhaled Micrometer-Sized Particles in Extrathoracic Airways of Children and Adolescents during Nose Breathing. Journal of Aerosol Science, 42(7):474-488.

Haddad G.G., Epstein R.A., Epstein M.A., Leistner H.L., Marino P.A., Mellins R.B. (1979). Maturation of Ventilation and Ventilatory Pattern in Normal Sleeping Infants. Journal of Applied Physiology: Respiratory, Environmental and Exercise Physiology, 46(5):998-1002.

Heyder J., Armbruster L., Gebhart J., Grein E., Stahlhofen W. (1975). Total Deposition of Aerosol Particles in the Human Respiratory Tract for Nose and Mouth Breathing. Journal of Aerosol Science, 6(5):311-328.

Hounam R.F., Black A., Walsh M. (1971). The Deposition of Aerosol Particles in the Nasopharyngeal Region of the Human Respiratory Tract. Journal of Aerosol Science, 2(1):47-61.

Hsu D.J., Chuang M.H. (2012). In-Vivo Measurements of Micrometer-Sized Particle Deposition in the Nasal Cavities of Taiwanese Adults. Aerosol Science & Technology, 46(6):631-638.

Kampa M., Castanas E. (2008). Human Health Effects of Air Pollution. Environmental Pollution, 151(2):362-367.

Kelly J., Asgharian B., Kimbell J., Wong B. (2004). Particle Deposition in Human Nasal Airway Replicas Manufactured by Different Methods. Part I: Inertial Regime Particles. Aerosol Science & Technology, 38(11):1063-1071.

Phalen R.F., Oldham M.J., Mautz W.J. (1989). Aerosol Deposition in the Nose as a Function of Body Size. Health Physics, 57:299-305.

Richards J.M., Alexander J.R., Shinebourne E.A., de Swiet M., Wilson A.J., Southall D.P. (1984). Sequential 22-Hour Profiles of Breathing Patterns and Heart Rate in 110 Full-Term Infants During Their First 6 Months of Life. Pediatrics, 74(5):763.

Rusconi F., Castagneto M. (1994). Reference Values for Respiratory Rate in the First 3 Years of Life. Pediatrics, 94(3):350.

Ruzycki C.A., Yang M., Chan H., Finlay W.H. (2017). Improved Prediction of Intersubject Variability in Extrathoracic Aerosol Deposition using Algebraic Correlations. Aerosol Science & Technology, 51(6):667-673.

Schroeter J.D., Garcia G.J.M., Kimbell J.S. (2011). Effects of Surface Smoothness on Inertial Particle Deposition in Human Nasal Models. Journal of Aerosol Science, 42(1):52-63.

Son J., Cho Y., Lee J. (2008). Effects of Air Pollution on Postneonatal Infant Mortality among Firstborn Infants in Seoul, Korea: Case-Crossover and Time-Series Analyses. Archives of Environmental & Occupational Health, 63(3):108-113.

Storey-Bishoff J., Noga M., Finlay W.H. (2008). Deposition of Micrometer-sized Aerosol Particles in Infant Nasal Airway Replicas. Journal of Aerosol Science, 39(12):1055-1065.

Swift D.L. (1991). Inspiratory Inertial Deposition of Aerosols in Human Nasal Airway Replicate Casts: Implication for the Proposed NCRP Lung Model. Radiation Protection Dosimetry, 38(1-3):29-34.

Walenga R.L., Tian G., Hindle M., Yelverton J., Dodson K., Longest P.W. (2014). Variability in Nose-to-lung Aerosol Delivery. Journal of Aerosol Science, 78:11-29.

Woodruff T.J., Grillo J., Schoendorf K.C. (1997). The Relationship between Selected Causes of Postneonatal Infant Mortality and Particulate Air Pollution in the United States. Environmental Health Perspectives, (6):608.

Yang M.Y., Ruzycki C., Verschuer J., Katsifis A., Eberl S., Wong K., Golshahi L., Brannan J.D., Finlay W.H., Chan H. (2017). Examining the Ability of Empirical Correlations to Predict Subject Specific In-Vivo Extrathoracic Aerosol Deposition during Tidal Breathing. Aerosol Science & Technology, 51(3):363-376.

Zhou Y., Guo M., Xi J., Irshad H., Cheng Y. (2014). Nasal Deposition in Infants and Children. Journal of Aerosol Medicine and Pulmonary Drug Delivery, 27(2):110-116.

Chapter 3: Scaling an Idealized Infant Nasal Airway Geometry to Mimic Inertial Filtration of Neonatal Nasal Airways

3.1 Introduction

The development of devices to aerosolize and deliver pharmaceutical aerosols is a challenging task. These devices must safely and effectively deliver aerosol medication to the target organs, usually the lungs. Delivering medication directly to the lungs provides rapid effect, allows relatively high doses to be delivered with low systemic dosing, and allows delivery of drugs with otherwise low bioavailability (Everard 2003). In order for aerosol particles to reach the lungs and serve their therapeutic purpose, they must first successfully traverse the extrathoracic airways.

An important design consideration for aerosol delivery devices is the diameter of aerosol particles produced by the device. Regional deposition, including extrathoracic deposition, is strongly dependent on particle diameter. The optimal particle diameter range for effective delivery to the lungs varies with delivery route (nasal vs oral) and the varying filtration characteristics of the extrathoracic airways with age. Further complicating the design of these devices are the fluid mechanics and particle physics associated with the devices and their interactions with the upper airway (DeHaan and Finlay 2004; Finlay and Martin 2007). These phenomena can be investigated using *in-vitro* testing of the device with an idealized extrathoracic airway. The idealized airway model is intended to mimic the average particle filtration properties of a population, while having a shape that is relatively easy to manufacture to high precision. Quantifying the aerosol that passes through the idealized airway model under specified flow conditions is representative of the aerosol that would reach the lungs when the device is used *in-vivo* under similar conditions.

Carefully designed idealized extrathoracic airways that are suited to manufacture using traditional high precision subtractive manufacturing methods have been described for oral inhalation of aerosols in adults (Grgic et al. 2004), and older children (Golshahi and Finlay 2012). Such idealized upper airways are an important tool used in the design and development of inhaled pharmaceutical aerosol products (e.g. Ciciliani et al. 2017; Sheth et al. 2017; Weers et al. 2015). However, an idealized airway model that is representative of extrathoracic deposition in very young children (i.e. neonates < 3 months of age) has not yet been presented. Infants are obligate nasal breathers (Sasaki et al. 1977), restricting the route of aerosol delivery to the lungs through the nasal passages. The deposition characteristics of infant nasal airways differ from those of adult oral airways. Thus, to design aerosol delivery devices for infants, an idealized infant nasal airway is

needed. Such an airway was developed by Javaheri et al. (2013) based on the airways of 10 infants aged 3-18 months studied earlier by Storey-Bishoff et al. (2008). However, we have shown in Chapter 2 that the neonatal population exhibits higher inertial deposition than the older infant population and thus the Javaheri et al. idealized infant geometry is not expected to mimic deposition in neonates. The success of scaling the adult Alberta Idealized Throat to mimic oral extrathoracic deposition in school-aged children (Golshahi and Finlay 2012) suggests that it may be possible to scale the Javaheri et al. idealized infant nasal geometry to mimic deposition in the younger neonatal population of infants.

In the present article, we seek to identify an appropriate scale factor to apply to the Javaheri et al. idealized infant geometry to give a geometry that accurately mimics average *in-vitro* nasal deposition of aerosols in upper airway replicas of neonates.

3.2 Methods

The deposition characteristics of a variety of isotropically scaled versions of an idealized nasal geometry were examined and compared to the deposition measured in the sample of nasal airway replicas of seven infants aged 5-79 days (Chapter 2) and a sample of ten nasal airway replicas of infants aged 3-18 months (Storey-Bishoff et al. 2008). A comparison of the infants studied in each sample is provided in Table 3.1.

Table 3.1: Comparison of neonatal/young infant (Chapter 2) and older infant (Storey-Bishoff et al. 2008) sample demographics and nasal replica characteristic diameters.

Neonates and Young Infants				Older Infants			
Sex	Age (days)	$D_{V/As}$ (mm)	D_{Garcia} (mm)	Sex	Age (months)	$D_{V/As}$ (mm)	D_{Garcia} (mm)
F	5	1.06	2.42	M	3	1.54	3.39
M	9	0.93	2.10	M	3	1.38	2.89
F	9	1.00	2.89	F	4	1.17	2.93
M	34	0.68	2.10	F	5	1.14	2.97
F	52	0.95	2.07	M	6	0.91	2.29
M	78	0.84	2.12	M	7	1.15	2.45
M	79	0.88	3.17	M	8	1.02	2.57
				M	16	1.36	3.95
				F	18	1.11	2.40
				M	15	1.26	3.61
Average:	38	0.91	2.41	Average:	8.5	1.20	2.95

D_{Garcia} data for older infant sample measured, calculated, and tabulated by Golshahi et al. 2010

3.2.1 Previously Developed Idealized Infant Geometry

An idealized infant airway was developed for older infants by Javaheri et al. (2013) based on the nasal airways of ten, 3-18 month old subjects studied by Storey-Bishoff et al. (2008). The primary features of each subject's upper airways were identified based on 24 cross-sections which were then used to create idealized cross-sections. The idealized airway is the result of using splines to transform the idealized cross-sections into a three-dimensional surface. The idealized airway begins at the nostril entrance and ends distal to the larynx. The left and right nasal cavities are symmetrical and are separated by a flat, centred septum. The turbinate region includes the three nasal meatuses, each one approximated as a meatus of regular cross-section. While maxillary sinuses are often observed to be connected to middle meatuses through a small opening, they have not been included in the idealized model since the opening is perpendicular to the expected flow direction and thus expected to minimally affect inertial deposition. Few simplifications are made in the pharynx region of the model as this portion of the airway is naturally less complicated. In this region, a disruption of the surface represents the oropharynx and then a constriction and offset of the axis of the airway represents the laryngopharynx. The model ends as a straight, circular pipe representing the upper trachea. The reader is referred to Javaheri et al. (2013) for a full description of this model and its simplification, and to Marieb and Hoehn (2007) for an in-depth description of the nasal structures and further discussion of the functions these structures perform.

In the quantification of inertial aerosol deposition in the infant models, Storey-Bishoff et al. (2008) identified the airway volume divided by the airway surface area as the characteristic diameter ($D_{V/As}$) which best collapsed intersubject variability onto a single curve. For this reason, the idealized geometry was created such that its characteristic diameter was equal to the average value of the realistic airways it is based on; i.e. $D_{V/As}$ = 1.20 mm for the older infants studied by Storey-Bishoff et al. (2008). Here we extend this previous work by scaling the previously developed idealized infant geometry down in size isotropically to a neonatal size using three scale factors as discussed below.

3.2.2 Scaling and Model Construction

The neonatal subjects considered here have smaller airways than the older infants upon which the Javaheri et al. (2013) idealized infant geometry was based. For this reason, a scale factor was identified by exploring several ratios of parameters between the neonatal and infant populations. One method for determining the scale factor uses the average characteristic diameter. The average $D_{V/As}$ in the neonate sample was 0.906 mm, 24 % smaller than the average infant model, indicating a possible scale factor of 0.76 be applied to the idealized infant model.

Alternatively, the characteristic diameter defined by Garcia et al. (2009), which relates the nasal airway to a circular pipe by comparing the resistance to flow, could be used. Briefly, the pressure drop (ΔP) through the nasal replica at specified constant flow rates (Q) is measured and fit to:

$$\Delta P = R_{nose} Q^{1.75} \tag{3.1}$$

where R_{nose} is the nasal resistance. The characteristic diameter is obtained by identifying the diameter of a smooth circular pipe that has the same resistance under turbulent flow, an equation for which is given by White (2008) based on the Blasius approximation for pipe friction and is

$$\Delta P = 0.241 L \rho^{3/4} \mu^{1/4} D^{-19/4} Q^{1.75} \tag{3.2}$$

Here, ρ is the density of the fluid flowing through the pipe, μ is the viscosity of the fluid, and L is the length of the pipe. Garcia et al. (2009) specify the length of the airway from the nostrils to the end of the septum as being the equivalent length of the pipe. Equating the resistance obtained from fitting pressure drop data for a specific nasal model using Equation 3.1 to the appropriate product of terms in Equation 3.2 and solving for D gives the characteristic diameter. The average 'Garcia diameter,' D_{Garcia}, of the neonate models was 2.41 mm while the idealized infant model has a D_{Garcia} of 3.52 mm indicating a scale factor of 0.68 should be applied. The average D_{Garcia} of the infant nasal replicas is 2.95 mm indicating a scale factor of 0.82. The discrepancy in Garcia diameter between the infant sample and the idealized geometry is likely due to reduced resistance in the idealized model due to convoluting features being removed. This is aligned with our findings in Chapter 2 that the Garcia diameter is a measure of both shape and size of the nasal airway. The idealized geometry has the same size ($D_{V/As}$) as the average infant airways studied by Storey-Bishoff et al. (2008) but with less convoluted features. Thus, the nasal resistance of the idealized airway is reduced resulting in a larger D_{Garcia}. Due to the nonlinear nature of the resistance of a duct as a function of its size, scale factors based on D_{Garcia} are expected to be only approximate estimates.

Scale factors were also identified based on ratios of anthropometric factors that include body mass and length, and head circumference. Body mass and body length data is given by the World Health Organization (WHO) growth charts (WHO 2009a, 2009b), while head circumference data is given by the Centers for Disease Control and Prevention (CDC) growth charts (CDC 2001). The average age of the neonate sample (38 days) was rounded to 1 month and the average age of the Storey-Bishoff et al. (2008) infant sample (8.5 months) was rounded to 9 months for obtaining values from the growth charts. Since body weight varies with the volume of the body, and volume is proportional to a length scale raised to the third power, a scale factor based on body weight was

identified as the third root of the ratio of average body weights. These scale factors and the data they are based on are listed in Table 3.2.

Table 3.2: Prospective scale factors to be applied to the idealized geometry and the data they are based on. Average age and characteristic diameters are from two samples of realistic nasal airways as given in Table 3.1: 1) Storey-Bishoff et al. (2008) for 10 infants (ages 3-18 months) and 2) the seven neonates (ages 5-79 days) studied in Chapter 2. Body mass and length, and head circumference are 50th percentile values (averaged for males and females) from WHO and CDC growth charts.

	Age	$D_{V/As}$ (mm)	D_{Garcia} (mm)	Body Mass (kg)	Body Length (cm)	Head Circumference (cm)
Neonates	1 month	0.91	2.41	4.40	54.5	37.6
Infants	9 months	1.20	2.95	8.55	71.0	44.6
Scale Factor	--	0.76	0.82	0.80	0.77	0.84

Scale factor for body mass is calculated as: $SF = (m_{neonate}/m_{infant})^{1/3}$ since mass scales with characteristic length cubed

These prospective scale factors rely on the assumption that the nasal cavity grows at the same rate as the whole infant. The validity of this assumption is unknown. However, based on the range of potential scale factors in Table 3.2, we chose to apply scale factors of 0.7 and 0.8 to the infant model to produce potential idealized neonate geometries. Additionally, a 0.6 scale model and the full size model was included in this study to broaden the range of sizes considered. Details of the characteristic dimensions of the scaled models are listed in Table 3.3.

Table 3.3: Characteristic diameters of the scaled idealized geometries. Scale of 1.0 is the original geometry.

Scale	$D_{V/As}$ (mm)	D_{Garcia} (mm)
0.6	0.72	2.04
0.7	0.84	2.27
0.8	0.96	2.62
1.0	1.20	3.52

The original idealized infant geometry was scaled isotropically in SOLIDWORKS (SOLIDWORKS 2016, Dassault Systèmes, Vélizy-Villacoublay, France); no changes were made to the airway or facial features in this process. The 0.7 and 0.8 scale models were printed using the same rapid prototyping machine (Eden 350V, Stratasys, Eden Prairie, MN, USA) and material (VeroGray, Stratasys) used to create the anatomic neonate airway models studied in Chapter 2, while the 0.6 and full-scale models were manufactured using direct metal laser sintering (Linear AMS, Livonia, Min, USA). We do not expect differences between these two manufacturing methods to significantly affect the deposition characteristics of the models due to the high resolution of both methods.

Indeed, we measured surface roughness (R_a) (Pocket Surf III, Mahr Federal, Providence, Rhode Island, USA) to be 1.9 μm for the VeroGray models and 3.3 μm for the metal models, indicating both have very smooth airway surfaces.

3.2.3 Deposition Measurements

To eliminate as many confounding variables as possible in the comparison of anatomic nasal replicas to the idealized geometry, the same experimental apparatus and method that was used to characterize deposition in the neonatal airway replicas was used to measure deposition in the idealized models (see §2.2.3). This allows a straightforward and direct comparison of deposition data points between idealized models to the sample population of neonatal infant replicas. Since the apparatus has already been explained in detail, it will only be briefly described here. Polydisperse aerosol of jojoba oil was generated using a 1-jet Collison nebulizer (MesaLabs, Butler, NJ, USA) and filled an exposure chamber into which two sampling lines extended, one of which was a blank line and to the other an airway replica was attached. The sampling lines (3/4" aluminum tubing, .0675" wall thickness) connected to a rigid piping system of 3/8" NPT stainless steel pipe in which a three way, quarter turn ball valve sent aerosol separately either through the blank or the model line. The sampled aerosol was then routed to an electrical low pressure impactor (ELPI) (Dekati Ltd., Kangasala, Finland) for measurement. The piping system included a branch for a constant supply of make-up air to satisfy the constant flow of 30 L/min into the ELPI and a branch leading to an ASL 5000 Breathing Simulator (IngMar Medical, Pittsburgh, PA, USA) which generated tidal flow profiles through the system. Flow rates in these branches were measured and monitored using mass flow meters (4043, TSI Inc., Shoreview, MN, USA). To eliminate the issue of the relatively large apparatus dead space in comparison to the tidal volume of the breathing patterns used, the exhaled portion was exhausted through a check valve near the ASL 5000. Thus, the deposition measurements reported here are for inspiratory deposition only; sampling lines were stagnant during the exhalation phase of the breath. Comparing the concentration of aerosol measured through the model line to that measured through the blank line gave the deposited fraction. Deposition was only considered for the particle size bins at which inertial deposition was dominant. These bins have aerodynamic diameter geometric centres between 0.53 and 5.54 μm.

The breathing patterns under which deposition was measured were the same as those the realistic nasal airway replicas were also tested, and are given in Table 3.4. All models were tested

using the five highest flow breathing patterns; breathing patterns one and two were only used in testing of the 0.6 scale model.

Table 3.4: Breathing pattern characteristic parameters and flow rates

Breathing Pattern	f (min^{-1})	V_t (mL)	Q (L/min)
1	30	19	1.78
2	50	21	3.28
3	89	17	4.73
4	50	45	7.03
5	75	40	9.38
6	55	68	11.69
7	45	100	14.06

f, respiratory rate; V_t, tidal volume;
Q, average inhalation flowrate = $(1/0.32)\cdot V_t \cdot f$

Three repeat measurements of each deposition data point were performed. Non-linear least squares fitting was performed, where necessary, in MATLAB (R2014a, MathWorks, Natick, MA, USA) using the Levenberg-Marquardt algorithm with unit weighting.

3.3 Results and Discussion

The primary function of the idealized geometry is to filter the correct proportion of specifically sized inertial particles at realistic inhalation flow rates. This can be evaluated by examining the measured deposition as a function of the impaction parameter. The impaction parameter, $d_a^2 Q$, has been described as a simplified (though dimensional) Stokes number for a single geometry where all constants are removed (Garcia et al. 2009). Since no consideration for airway size or shape is included in this parameter, it also displays how substantial the variability in deposition is within a population. The goal of the idealized geometry is to provide average deposition and so its data points should lie near the middle of the cloud of deposition data points. Figure 3.1 compares the measured deposition in the scaled idealized models to the deposition of the neonatal and infant airway replicas as a function of the impaction parameter.

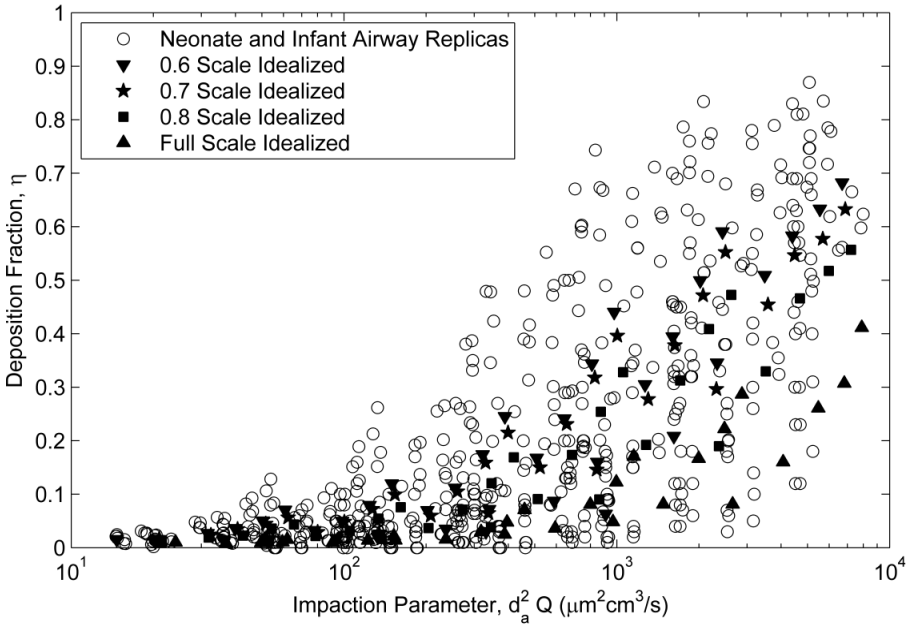

Figure 3.1: Comparison of deposition measured in four different sizes of the idealized geometry and the deposition measured in infant nasal replicas based on infants aged 5 days to 18 months

The significant spread of the deposition data in Figure 3.1 and the fact that the scaled idealized geometries lie in different areas of the data cloud indicate that varied sizes of the idealized geometry can be used to target different subsets of the sample. This becomes readily apparent when the total nasal replica deposition data is split in two sets, with one set consisting of the neonatal and young infant (5 to 79 days old) nasal replicas and the other consisting of the set of infant (3 to 18 months old) nasal replicas studied by Storey-Bishoff et al. (2008). Figure 3.2 shows that the 0.6 scaled geometry fits average deposition in neonatal (<3 month old) subjects, while Figure 3.3 shows that the 0.8 scaled geometry fits the older (3-18 month old) infants of the Storey-Bishoff et al. study.

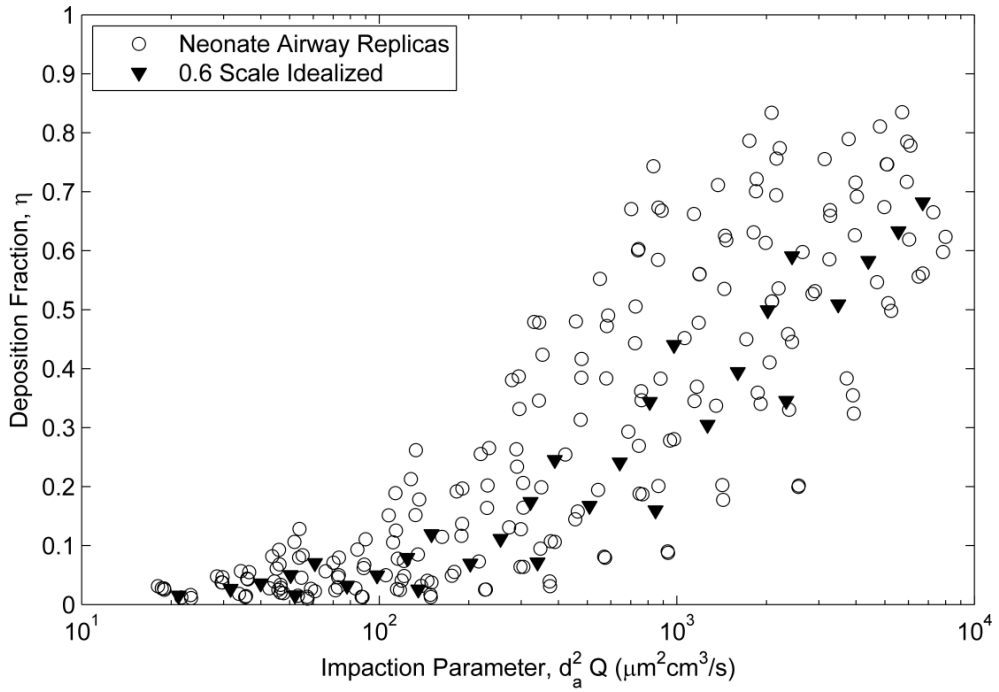

Figure 3.2: Comparison of neonatal nasal deposition to 0.6 scale idealized model deposition

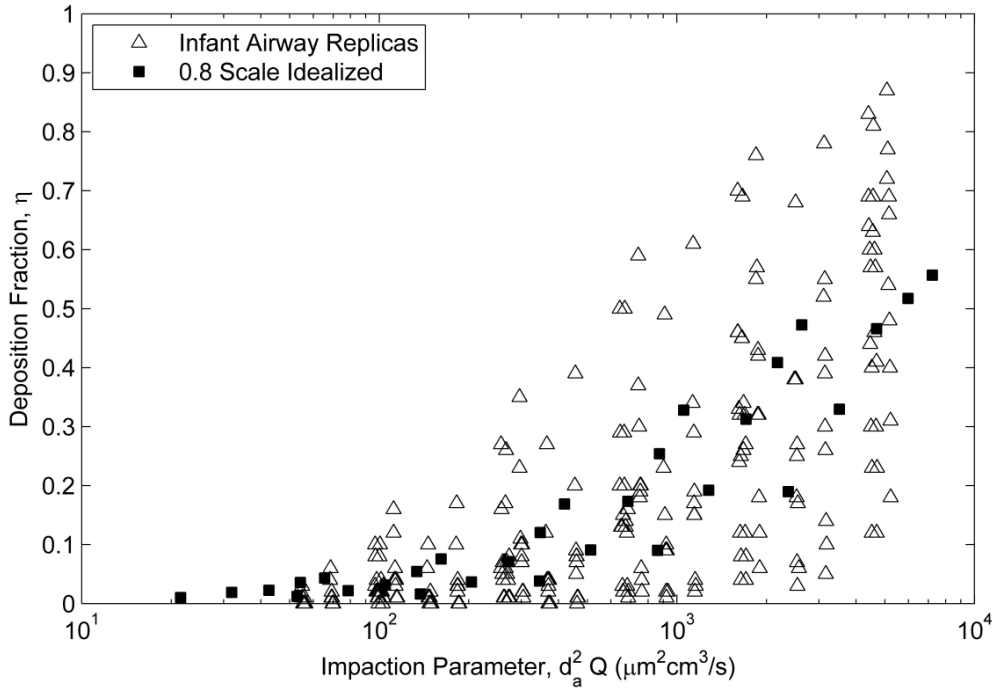

Figure 3.3: Comparison of infant nasal deposition to 0.8 scale idealized model deposition

The age specific nature of the scale factor can be examined quantitatively using statistical comparison of regression coefficients. Linear regression was used to fit the deposition cloud of each idealized model as well as the replica samples. Since deposition was not measured under breathing patterns 1 and 2 in all idealized models, regressions were done using deposition data from breathing patterns 3 through 7 only. To test if regression lines were different, t-tests against regression coefficients were used (Zar 1984). No statistical difference in slope nor elevation ($p > 0.01$) was found between the regression line of the neonate replicas and the regression line for the 0.6 scale idealized geometry.

The null hypothesis (that regression coefficients are the same) was similarly not rejected ($p > 0.01$) for the slope and elevation of the regression lines for the infant nasal airway replicas versus the 0.8 scale idealized geometry. This latter observation is in contrast with the results of Javaheri et al. 2013 where the full scale idealized geometry (i.e. a scale factor of 1.0) was found to match the average of the infant sample. We believe that this difference is due to several improvements in the present experimental design as compared to the apparatus used by Javaheri et al. 2013. In particular, we have replaced the custom built pulmonary waveform generator with a high accuracy breathing simulator (ASL 5000), used a more accurate mass flow meter for monitoring makeup flow to the ELPI (rotameter replaced by TSI 4043 mass flowmeter), and identified an instability in the building compressed air source that made it unsuitable for use as a source for the ELPI makeup air (we instead used clean, dry compressed air from a large compressed gas cylinder). These improvements in the experimental apparatus likely eliminated a systematic error present in the apparatus used by Javaheri et al. (2013) which may have artificially inflated their deposition measurements.

Of further interest is the relative size of the two models that most closely fit the two subset populations i.e. younger (<3 months old) vs older (3-18 months old) infants. The present results indicate that a 0.8 scale model more accurately captures average deposition in the older infant replicas (with average age of 9 months) than the full scale model. Therefore, to mimic average deposition in the younger (<3 months) replicas, the scale factors presented in Table 2 should be applied to the 0.8 scale model rather than the full scale model. We have found that a scale factor of 0.75 should be applied to the geometry that correctly predicts the older (Storey-Bishoff et al. 2008) infant deposition data. Applying a scale factor of 0.75 to the 0.8 scale model results in a 0.6 scale of the original geometry. This is in good agreement with the prospective scale factors based on characteristic diameter ($D_{V/As}$) and body length seen in Table 3.2.

The original, full scale model may potentially mimic a different subset of the infant population. The full scale model is equivalent to a 1.25 scale of the 0.8 scale model. Using this equivalent scale factor in a reverse fashion with Table 3.2, a 50th percentile body length and average age can then be identified using the WHO growth charts. That is, a scale factor of 1.25 would be identified as appropriate if attempting to create an idealized geometry for a sample with an average body length of 89 cm. This corresponds to 50th percentile body lengths of male and female infants aged 26 and 27 months old respectively. Thus a 1.0 scale model may mimic toddler nasal filtration, however this remains to be verified.

3.3.1 Non-Dimensional Analysis

The agreement seen between the projected scale factors based on characteristic diameter ($D_{V/As}$) and body length and the resulting scale factor of neonate to infant idealized geometries suggests the possibility of identifying an appropriate scale factor for generating a model representative of the average deposition expected in a specific subset of the infant population. It may be useful to know the deposition characteristics of this model prior to building it or to identify the characteristic diameter of a model that would produce a given filtration at certain conditions. Thus, a predictive equation describing the deposition characteristics of these models would be useful. Since the four models tested in this study are geometrically similar, dimensional analysis dictates that a single equation should capture deposition in all four sizes and can be found if the correct non-dimensional groups are used, which here includes the Stokes and Reynolds numbers. While we have previously identified an equation describing deposition in the realistic neonate airway replicas that is also a function of the Euler number (a dimensionless pressure drop) in addition to the Reynolds and Stokes numbers, this equation is not applicable here since the shape of the idealized airway differs from the realistic replicas and the dependence of deposition on the Euler number was attributed, in Chapter 2, to shape differences between the realistic replicas. Since the scaled idealized models are geometrically similar, these shape differences are not present and thus the Euler number is not required. Besides, if the Euler number was included in the predictive equation, an estimate of the replica nasal resistance would be required, further complicating the application of this model.

As seen in Figure 3.4, a predictive correlation based on least squares fitting of Reynolds and Stokes numbers accurately describes deposition in all examined scales of the model. This equation can be used to describe deposition in this geometry for scales inclusive of 0.6 to full scale and is as follows:

$$\eta = 1 - \left(\frac{2.508 \cdot 10^6}{2.508 \cdot 10^6 - Stk^{1.0933} Re^{1.3744}} \right)^{0.3228} \tag{3.3}$$

where, the Stokes and Reynolds numbers follow their standard definitions (see Chapter 2, equations 2.5 and 2.6, respectively) and are evaluated using $D_{V/As}$ for the length scale.

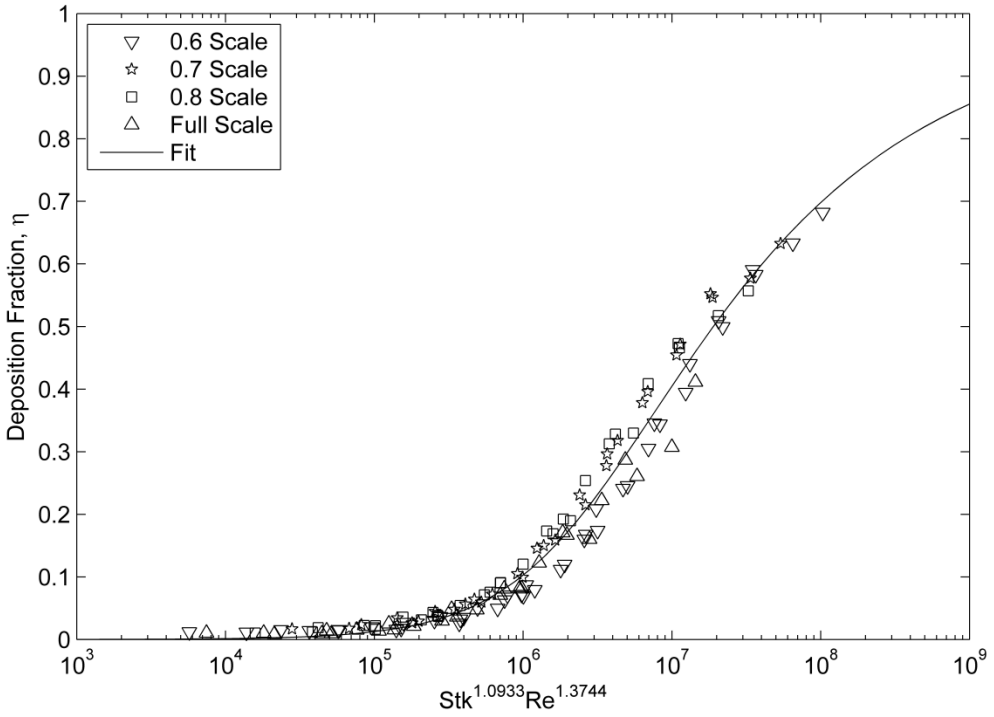

Figure 3.4: Deposition in scaled models of the idealized infant nasal airway as a function of non-dimensional deposition parameter. Fit defined in Equation 3.3, evaluated with characteristic diameter $D=V/A_S$, r^2 = 0.97

3.4 Conclusions

The ability to scale a previously developed infant idealized nasal airway to produce an idealized neonatal nasal airway has been explored through in-vitro measurements. Ratios of the airway characteristic diameters of neonates (ages 0-3 months) and infants (ages 3-18 months) and of 50th percentile body lengths for the average age of the subjects correctly provided appropriate scale factors (0.76 and 0.77, respectively) to be applied to the infant geometry. Isotropically scaling the infant geometry produced an airway geometry with the same average deposition properties as the sample of seven realistic nasal airway replicas based on infants aged 5 to 79 days old. Non-dimensional analysis of the deposition data yielded an equation capable of describing the deposition in this geometry for all scales of the geometry we have tested. The scaled idealized infant nasal airway may be useful in future *in-vitro* experiments of aerosol delivery to the lungs of neonatal and young infants.

3.5 Works Cited

Centers for Disease Control and Prevention. (2001). Data table of infant head circumference-for-age charts. Last modified August 24, 2001, https://www.cdc.gov/growthcharts/html_charts/hcageinf.htm

Ciciliani A., Langguth P., Wachtel H. (2017). In Vitro Dose Comparison of Respimat Inhaler with Dry Powder Inhalers for COPD Maintenance Therapy. International Journal of COPD, 12:1565-1577.

DeHaan W.H., Finlay W.H. (2004). Predicting Extrathoracic Deposition from Dry Powder Inhalers. Journal of Aerosol Science, 35:309-331.

Everard M.L. (2003). Inhalation Therapy for Infants. Advanced Drug Delivery Reviews, 55(7):869-878.

Finlay, W.H., Martin, A.R. (2007). Modeling of Aerosol Deposition with Interface Devices. Journal of Aerosol Medicine: Deposition, Clearance, and Effects in the Lung, 20:S19-S26.

Garcia G.J., Tewksbury E.W., Wong B.A., Kimbell J.S. (2009). Interindividual Variability in Nasal Filtration as a Function of Nasal Cavity Geometry. Journal of Aerosol Medicine and Pulmonary Drug Delivery, 22(2):139-155.

Golshahi L., Finlay W.H., Olfert J.S., Thompson R.B., Noga M.L. (2010). Deposition of Inhaled Ultrafine Aerosols in Replicas of Nasal Airways of Infants. Aerosol Science & Technology, 44(9):741-752.

Golshahi L., Finlay W.H. (2012). An Idealized Child Throat that Mimics Average Pediatric Oropharyngeal Deposition. Aerosol Science and Technology, 46(5):i-iv.

Grgic B., Finlay W.H., Heenan A.F. (2004). Regional Aerosol Deposition and Flow Measurements in an Idealized Mouth and Throat. Journal of Aerosol Science, 35:21-32.

Javaheri E., Golshahi L., Finlay W.H. (2013). An Idealized Geometry that Mimics Average Infant Nasal Airway Deposition. Journal of Aerosol Science, 55:137-148.

Marieb E.N., Hoehn K. (2007). Human Anatomy & Physiology, 7th Edition. Pearson Benjamin Cummings, San Francisco.

Sasaki C.T., Levine P.A., Laitman J.T., Crelin E.S., J. (1977). Postnatal Descent of the Epiglottis in Man. A Preliminary Report. Archives of Otolaryngology, 103(3):169-171.

Sheth P., Grimes M.R., Stein S.W., Myrdal P.B. (2017). Impact of Droplet Evaporation Rate on Resulting In Vitro Performance Parameters of Pressurized Metered Dose Inhalers. International Journal of Pharmaceutics, 528:360-371.

Storey-Bishoff J., Noga M., Finlay W.H. (2008). Deposition of Micrometer-Sized Aerosol Particles in Infant Nasal Airway Replicas. Journal of Aerosol Science, 39(12):1055-1065.

Weers J.G., Clark A.R., Rao N., Ung K., Haynes A., Khindri S.K., Perry S.A., Machineni S., Colthorpe P. (2015). In Vitro-In Vivo Correlations Observed with Indacaterol-Based Formulations Delivered with the Breezhaler. Journal of Aerosol Medicine and Pulmonary Drug Delivery, 28(4):268-280.

White F.M. (2008). Fluid Mechanics, 6th Edition. McGraw-Hill Higher Education, Boston.

World Health Organization. (2009a). Birth to 24 months: Boys Length-for-Age and Weight-for-Age Percentiles. Last modified November 1, 2009, https://www.cdc.gov/growthcharts/data/who/GrChrt_Boys_24LW_100611.pdf

World Health Organization. (2009b). Birth to 24 months: Girls Length-for-Age and Weight-for-Age Percentiles. Last modified November 1, 2009, https://www.cdc.gov/growthcharts/data/who/GrChrt_Girls_24LW_9210.pdf

Zar J.H. (1984). Biostatistical Analysis, 2nd Edition. Prentice-Hall, Englewood Cliffs.

Chapter 4: Conclusions

4.1 Summary of Work

This thesis has focused on the quantification and description of the inertial filtration properties of neonatal infant nasal airways. The presented work eliminates a gap in our previous understanding of human extrathoracic deposition properties; namely, a description of filtration within the youngest individuals has been formulated. This led to the identification of a suitable scaling of the idealized infant nasal airway to mimic deposition in the younger population. It is hoped that this work will empower future research regarding the successful delivery of therapeutic aerosols to the lungs of the most vulnerable members of our society.

The first primary goal of this project was achieved in Chapter 2 of this thesis. Nasal airway replicas based on CT scan images of seven infants aged 5-79 days were constructed using three-dimensional printing. Deposition of aerosols in these models was measured under simulated tidal inhalation profiles and compared to deposition previously measured in older infants between the ages of 3 and 18 months. Increased deposition was measured in the neonatal population. Further, the correlation which described nasal deposition in older infants was found not to satisfactorily describe deposition in the younger population. While that correlation was close to describing the average deposition it failed to collapse the intersubject variability in the younger population. This was attributed to extrapolation of the correlation to geometries outside the size and age range for which it was developed. Satisfactory collapse of intersubject variability was achieved through non-linear least squares fitting with non-dimensional Reynolds, Stokes, and Euler numbers as input variables. The Euler number, a non-dimensional pressure drop, has not been required to describe deposition in older populations before; its necessity here is thought to be a result of increased intersubject variability in the younger population. A relatively new method of using *in-vitro* deposition equations to predict a population's *in-vivo* deposition distribution (as opposed to subject specific deposition) was explored based on recently observed sensitivity of deposition equations to extrapolation. Through a propagation of error approach, the average and expected variance of filtration was identified for specific conditions. The method can be followed for different aerosol distributions or inhalation flowrates.

Finding that neonatal deposition was higher than in older infants, it became clear that our previously developed idealized infant nasal airway developed for older infants would not properly mimic average deposition in the younger population. Thus an appropriate scale factor was identified to apply to the full scale idealized infant model to produce a model with the correct

deposition properties. This is the second primary goal of the thesis and was accomplished in chapter three. Scale factors were predicted based on the average characteristic diameters of the two airway replica samples and based on 50th percentile demographic data corresponding to the average age of the subjects constituting each sample. The original idealized model was scaled by factors of 0.7 and 0.8 and produced using the same equipment used to produce the realistic nasal replicas. The deposition properties of these models, and a previously constructed 0.6 scale and the original full scale model, were measured using the same experimental method used to quantify deposition in the nasal replica models. The 0.6 scale model was found to mimic average deposition in the neonatal population while the 0.8 model was found to more accurately mimic deposition in the infant population opposed to the originally thought full scale model. Scale factors identified based on sample average airway characteristic diameter (airway volume divided by surface area) and 50th percentile body lengths agreed with the scale factor identified through experiment. Finally, non-linear least squares fitting of the deposition data in the idealized models produced an equation based on Reynolds and Stokes numbers which described deposition well for all scales of the idealized model considered here.

4.2 Future Work

While this work represents a significant step forward in the field of extrathoracic deposition of aerosol particles, significant work remains. The filtration properties of extrathoracic airways cannot be extrapolated from the inertial regime to the diffusion regime since the governing mechanisms are drastically different. Thus, the deposition of ultrafine particles in the newly developed neonatal models should be investigated, especially for evaluating the risks associated with atmospheric aerosol exposure. Another mode of deposition which remains largely unstudied in all ages is deposition under expiration due to the difficulty of reproducing the appropriate inlet condition; upon the development of a method to study deposition under exhalation these measurements should be performed in the neonatal nasal airway replicas. Also, intersubject variability has received much attention yet the notion of intrasubject variability remains unstudied. If possible, multiple airway replicas of an individual based on CT imaging at multiple stages of life would provide insight to how the filtration properties of an individual evolves with age. This could perhaps account for some of the observed intersubject variability observed in studies of multiple individuals who naturally develop at different rates. One concern with in-vitro deposition measurements is the roughness of the nasal replica models. A definitive study identifying a maximum acceptable build layer or voxel resolution for extrathoracic airway models would be useful. Finally, corroboration of these *in-vitro* results through in-vivo measurements would be

welcomed. This data is not expected to be available in the near future due to the risks and difficulty of *in-vivo* techniques for infants. The development of new methods with no perceived health risks may enable these measurements.

Bibliography

Becquemin M.H., Swift D.L., Bouchikhi A., Roy M., Teillac A. (1991). Particle Deposition and Resistance in the Noses of Adults and Children. The European Respiratory Journal, 4(6):694-702.

Bennett W.D., Zeman K.L., Jarabek A.M. (2008). Nasal Contribution to Breathing and Fine Particle Deposition in Children versus Adults. Journal of Toxicology & Environmental Health, 71(3):227-237.

Çengel Y.A., Cimbala J.M. (2010). Fluid mechanics: Fundamentals and Applications. McGraw-Hill Higher Education, Boston.

Centers for Disease Control and Prevention. (2001). Data table of infant head circumference-for-age charts. Last modified August 24, 2001, https://www.cdc.gov/growthcharts/html_charts/hcageinf.htm

Cheng Y.S., Smith S.M., Yeh, H.C. (1995). Deposition of Ultrafine Aerosols and Thoron Progeny in Replicas of Nasal Airways of Young Children. Aerosol Science and Technology, 23(4):541-552.

Cheng Y.S. (2003). Aerosol Deposition in the Extrathoracic Region. Aerosol Science & Technology, 37(8):659.

Ciciliani A., Langguth P., Wachtel H. (2017). In Vitro Dose Comparison of Respimat Inhaler with Dry Powder Inhalers for COPD Maintenance Therapy. International Journal of COPD, 12:1565-1577.

DeHaan W.H., Finlay W.H. (2004). Predicting Extrathoracic Deposition from Dry Powder Inhalers. Journal of Aerosol Science, 35:309-331.

Estol P., Priz H., Pintos L., Nieto F., Simini F. (1988). Assessment of Pulmonary Dynamics in Normal Newborns: A Pneumotachographic Method. Journal of Perinatal Medicine, 16(3):183-192.

Everard M.L. (2003). Inhalation Therapy for Infants. Advanced Drug Delivery Reviews, 55(7):869-878.

Finlay, W.H., Martin, A.R. (2007). Modeling of Aerosol Deposition with Interface Devices. Journal of Aerosol Medicine: Deposition, Clearance, and Effects in the Lung, 20:S19-S26.

Fuchs O., Latzin P., Thamrin C., Stern G., Frischknecht P., Singer F., Kieninger E., Proietti E., Riedel T., Frey U. (2011). Normative Data for Lung Function and Exhaled Nitric Oxide in Unsedated Healthy Infants. The European Respiratory Journal, 37(5):1208-1216.

Garcia G.J., Tewksbury E.W., Wong B.A., Kimbell J.S. (2009). Interindividual Variability in Nasal Filtration as a Function of Nasal Cavity Geometry. Journal of Aerosol Medicine and Pulmonary Drug Delivery, 22(2):139-155.

Golshahi L., Finlay W.H., Olfert J.S., Thompson R.B., Noga M.L. (2010). Deposition of Inhaled Ultrafine Aerosols in Replicas of Nasal Airways of Infants. Aerosol Science & Technology, 44(9):741-752.

Golshahi L., Noga M.L., Thompson R.B., Finlay W.H. (2011). In Vitro Deposition Measurement of Inhaled Micrometer-Sized Particles in Extrathoracic Airways of Children and Adolescents during Nose Breathing. Journal of Aerosol Science, 42(7):474-488.

Golshahi L., Finlay W.H. (2012). An Idealized Child Throat that Mimics Average Pediatric Oropharyngeal Deposition. Aerosol Science and Technology, 46(5):i-iv.

Grgic B., Finlay W.H., Heenan A.F. (2004). Regional Aerosol Deposition and Flow Measurements in an Idealized Mouth and Throat. Journal of Aerosol Science, 35:21-32.

Haddad G.G., Epstein R.A., Epstein M.A., Leistner H.L., Marino P.A., Mellins R.B. (1979). Maturation of Ventilation and Ventilatory Pattern in Normal Sleeping Infants. Journal of Applied Physiology: Respiratory, Environmental and Exercise Physiology, 46(5):998-1002.

Heyder J., Armbruster L., Gebhart J., Grein E., Stahlhofen W. (1975). Total Deposition of Aerosol Particles in the Human Respiratory Tract for Nose and Mouth Breathing. Journal of Aerosol Science, 6(5):311-328.

Hounam R.F., Black A., Walsh M. (1971). The Deposition of Aerosol Particles in the Nasopharyngeal Region of the Human Respiratory Tract. Journal of Aerosol Science, 2(1):47-61.

Hsu D.J., Chuang M.H. (2012). In-Vivo Measurements of Micrometer-Sized Particle Deposition in the Nasal Cavities of Taiwanese Adults. Aerosol Science & Technology, 46(6):631-638.

Itoh H., Smaldone G.C., Swift D.L., Wagner H.N. (1985). Mechanisms of Aerosol Deposition in a Nasal Model. Journal of Aerosol Science, 16(6):529-534.

Janssens H.M., de Jongste J.C., Fokkens W.J., Robben S.G.F., Wouters K., Tiddens H.A.W.M. (2001). The Sophia Anatomical Infant Nose-Throat (Saint) Model: A Valuable Tool to Study Aerosol Deposition in Infants. Journal of Aerosol Medicine, 14(4):433-441.

Javaheri E., Golshahi L., Finlay W.H. (2013). An Idealized Geometry that Mimics Average Infant Nasal Airway Deposition. Journal of Aerosol Science, 55:137-148.

Kampa M., Castanas E. (2008). Human Health Effects of Air Pollution. Environmental Pollution, 151(2):362-367.

Kelly J., Asgharian B., Kimbell J., Wong B. (2004). Particle Deposition in Human Nasal Airway Replicas Manufactured by Different Methods. Part I: Inertial Regime Particles. Aerosol Science & Technology, 38(11):1063-1071.

Marieb E.N., Hoehn K. (2007). Human Anatomy & Physiology, 7th Edition. Pearson Benjamin Cummings, San Francisco.

Minocchieri S., Burren J.M., Bachmann M.A., Stern G., Wildhaber J., Buob S., Schindel R., Kraemer R., Frey U.P., Nelle M. (2008). Development of the Premature Infant Nose Throat-Model (PrINT-Model): An Upper Airway Replica of a Premature Neonate for the Study of Aerosol Delivery. Pediatric Research 64(2):141-146.

Phalen R.F., Oldham M.J., Mautz W.J. (1989). Aerosol Deposition in the Nose as a Function of Body Size. Health Physics, 57:299-305.

Richards J.M., Alexander J.R., Shinebourne E.A., de Swiet M., Wilson A.J., Southall D.P. (1984). Sequential 22-Hour Profiles of Breathing Patterns and Heart Rate in 110 Full-Term Infants During Their First 6 Months of Life. Pediatrics, 74(5):763.

Rusconi F., Castagneto M. (1994). Reference Values for Respiratory Rate in the First 3 Years of Life. Pediatrics, 94(3):350.

Ruzycki C.A., Yang M., Chan H., Finlay W.H. (2017). Improved Prediction of Intersubject Variability in Extrathoracic Aerosol Deposition using Algebraic Correlations. Aerosol Science & Technology, 51(6):667-673.

Sasaki C.T., Levine P.A., Laitman J.T., Crelin E.S., J. (1977). Postnatal Descent of the Epiglottis in Man. A Preliminary Report. Archives of Otolaryngology, 103(3):169-171.

Schroeter J.D., Garcia G.J.M., Kimbell J.S. (2011). Effects of Surface Smoothness on Inertial Particle Deposition in Human Nasal Models. Journal of Aerosol Science, 42(1):52-63.

Sheth P., Grimes M.R., Stein S.W., Myrdal P.B. (2017). Impact of Droplet Evaporation Rate on Resulting In Vitro Performance Parameters of Pressurized Metered Dose Inhalers. International Journal of Pharmaceutics, 528:360-371.

Son J., Cho Y., Lee J. (2008). Effects of Air Pollution on Postneonatal Infant Mortality among Firstborn Infants in Seoul, Korea: Case-Crossover and Time-Series Analyses. Archives of Environmental & Occupational Health, 63(3):108-113.

Stein S.W., Thiel C.G. (2017). The History of Therapeutic Aerosols: A Chronological Review. Journal of Aerosol Medicine & Pulmonary Drug Delivery, 30(1):20-41.

Storey-Bishoff J., Noga M., Finlay W.H. (2008). Deposition of Micrometer-sized Aerosol Particles in Infant Nasal Airway Replicas. Journal of Aerosol Science, 39(12):1055-1065.

Swift D.L. (1991). Inspiratory Inertial Deposition of Aerosols in Human Nasal Airway Replicate Casts: Implication for the Proposed NCRP Lung Model. Radiation Protection Dosimetry, 38(1-3):29-34.

Walenga R.L., Tian G., Hindle M., Yelverton J., Dodson K., Longest P.W. (2014). Variability in Nose-to-lung Aerosol Delivery. Journal of Aerosol Science, 78:11-29.

Weers J.G., Clark A.R., Rao N., Ung K., Haynes A., Khindri S.K., Perry S.A., Machineni S., Colthorpe P. (2015). In Vitro-In Vivo Correlations Observed with Indacaterol-Based Formulations Delivered with the Breezhaler. Journal of Aerosol Medicine and Pulmonary Drug Delivery, 28(4):268-280.

White F.M. (2008). Fluid Mechanics, 6th Edition. McGraw-Hill Higher Education, Boston.

Woodruff T.J., Grillo J., Schoendorf K.C. (1997). The Relationship between Selected Causes of Postneonatal Infant Mortality and Particulate Air Pollution in the United States. Environmental Health Perspectives, (6):608.

World Health Organization. (2009a). Birth to 24 months: Boys Length-for-Age and Weight-for-Age Percentiles. Last modified November 1, 2009, https://www.cdc.gov/growthcharts/data/who/GrChrt_Boys_24LW_100611.pdf

World Health Organization. (2009b). Birth to 24 months: Girls Length-for-Age and Weight-for-Age Percentiles. Last modified November 1, 2009, https://www.cdc.gov/growthcharts/data/who/GrChrt_Girls_24LW_9210.pdf

Yang M.Y., Ruzycki C., Verschuer J., Katsifis A., Eberl S., Wong K., Golshahi L., Brannan J.D., Finlay W.H., Chan H. (2017). Examining the Ability of Empirical Correlations to Predict Subject Specific In-Vivo Extrathoracic Aerosol Deposition during Tidal Breathing. Aerosol Science & Technology, 51(3):363-376.

Zar J.H. (1984). Biostatistical Analysis, 2nd Edition. Prentice-Hall, Englewood Cliffs.

Zeman K.L., Balcazar J.R., Fuller F., Donn K.H., Boucher R.C., Bennett W.D., Donaldson S.H. (2017). A Trans-Nasal Aerosol Delivery Device for Efficient Pulmonary Deposition. Journal of Aerosol Medicine & Pulmonary Drug Delivery, 30(4):223-229.

Zhou Y., Guo M., Xi J., Irshad H., Cheng Y. (2014). Nasal Deposition in Infants and Children. Journal of Aerosol Medicine and Pulmonary Drug Delivery, 27(2):110-116.

Appendix A: Nasal Replica Deposition Data

Table A.1: Subject 1 Deposition Data

Q (L/min)	d_a (μm)	η (%)
1.72	0.53	0.56 ± 0.22
	0.83	0.61 ± 0.24
	1.34	0.86 ± 0.27
	2.12	1.54 ± 0.28
	3.34	2.8 ± 0.31
	5.54	4.06 ± 1.78
3.35	0.53	0.82 ± 0.15
	0.83	0.92 ± 0.14
	1.34	1.68 ± 0.12
	2.12	4.43 ± 0.13
	3.34	10.46 ± 0.11
	5.54	18.03 ± 0.59
4.65	0.53	1.22 ± 0.16
	0.83	1.51 ± 0.15
	1.34	3.17 ± 0.09
	2.12	9.49 ± 0.03
	3.34	20.12 ± 0.22
	5.54	33.05 ± 0.32
7.27	0.53	1.82 ± 0.08
	0.83	2.77 ± 0.09
	1.34	7.32 ± 0.17
	2.12	19.45 ± 0.24
	3.34	33.72 ± 0.32
	5.54	38.36 ± 1.27
9.19	0.53	2.76 ± 0.2
	0.83	4.99 ± 0.37
	1.34	13.1 ± 0.62
	2.12	29.33 ± 0.7
	3.34	44.98 ± 0.73
	5.54	54.68 ± 2.24
11.78	0.53	4.56 ± 0.37
	0.83	8.51 ± 0.42
	1.34	19.88 ± 0.58
	2.12	38.31 ± 0.73
	3.34	53.62 ± 0.46
	5.54	61.91 ± 1.09
14.19	0.53	5.65 ± 0.22
	0.83	11.48 ± 0.27
	1.34	25.44 ± 0.39
	2.12	45.2 ± 0.51
	3.34	59.79 ± 0.31
	5.54	66.52 ± 1.1

Table A.2: Subject 2 Deposition Data

Q (L/min)	d_a (μm)	η (%)
1.77	0.53	1.27 ± 0.02
	0.83	1.4 ± 0.11
	1.34	1.8 ± 0.09
	2.12	3.34 ± 0.34
	3.34	6.93 ± 0.46
	5.54	13.4 ± 1.21
3.18	0.53	1.78 ± 0.25
	0.83	1.94 ± 0.26
	1.34	3.21 ± 0.27
	2.12	9.47 ± 0.22
	3.34	23.95 ± 0.25
	5.54	37.42 ± 0.61
4.08	0.53	2.53 ± 0.12
	0.83	2.83 ± 0.13
	1.34	4.84 ± 0.37
	2.12	16.44 ± 0.51
	3.34	34.66 ± 0.6
	5.54	51.43 ± 0.99
6.39	0.53	3.75 ± 0.06
	0.83	4.99 ± 0.12
	1.34	13.7 ± 0.39
	2.12	38.48 ± 0.59
	3.34	55.99 ± 0.57
	5.54	66.88 ± 0.54
7.78	0.53	4.3 ± 0.12
	0.83	6.77 ± 0.21
	1.34	20.2 ± 0.65
	2.12	47.22 ± 0.7
	3.34	62.54 ± 0.82
	5.54	71.57 ± 1.17
9.94	0.53	6.82 ± 0.13
	0.83	12.56 ± 0.2
	1.34	33.18 ± 0.36
	2.12	60.29 ± 1.06
	3.34	72.15 ± 1.33
	5.54	74.64 ± 1.15
11.89	0.53	8.37 ± 0.44
	0.83	17.82 ± 0.64
	1.34	42.37 ± 0.74
	2.12	66.79 ± 0.53
	3.34	77.4 ± 1.41
	5.54	77.82 ± 1.2

Table A.3: Subject 3 Deposition Data

Q (L/min)	d_a (μm)	η (%)
1.75	0.53	0.27 ± 0.09
	0.83	0.18 ± 0.02
	1.34	0.44 ± 0.03
	2.12	0.95 ± 0.18
	3.34	1.62 ± 0.33
	5.54	5.26 ± 1.46
3.41	0.53	0.77 ± 0.11
	0.83	0.82 ± 0.09
	1.34	0.96 ± 0.15
	2.12	1.63 ± 0.13
	3.34	3.25 ± 0.14
	5.54	7.04 ± 1.23
5.01	0.53	1.11 ± 0.13
	0.83	1.01 ± 0.08
	1.34	1.3 ± 0.1
	2.12	3.12 ± 0.16
	3.34	8.78 ± 0.43
	5.54	20.18 ± 0.44
7.62	0.53	1.28 ± 0.2
	0.83	1.33 ± 0.2
	1.34	2.54 ± 0.24
	2.12	8.13 ± 0.29
	3.34	20.28 ± 0.65
	5.54	35.49 ± 1.27
10.02	0.53	2.03 ± 0.11
	0.83	2.63 ± 0.14
	1.34	6.41 ± 0.19
	2.12	18.81 ± 0.26
	3.34	35.94 ± 0.42
	5.54	51.11 ± 2.02
12.68	0.53	2.68 ± 0.2
	0.83	4.05 ± 0.21
	1.34	10.74 ± 0.25
	2.12	27.83 ± 0.21
	3.34	45.87 ± 0.5
	5.54	55.62 ± 0.95
15.31	0.53	2.44 ± 0.11
	0.83	4.9 ± 0.13
	1.34	14.47 ± 0.17
	2.12	34.53 ± 0.22
	3.34	52.67 ± 0.38
	5.54	59.78 ± 1.13

Table A.4: Subject 4 Deposition Data

Q (L/min)	d_a (μm)	η (%)
1.77	0.53	1.91 ± 0.26
	0.83	1.63 ± 0.5
	1.34	2.05 ± 0.23
	2.12	3.17 ± 0.27
	3.34	5.77 ± 0.45
	5.54	15.78 ± 1.32
3.16	0.53	2.14 ± 0.07
	0.83	1.98 ± 0.22
	1.34	2.65 ± 0.16
	2.12	7.14 ± 0.16
	3.34	18.39 ± 0.13
	5.54	30.68 ± 0.48
4.00	0.53	2.76 ± 0.22
	0.83	2.5 ± 0.41
	1.34	4.07 ± 0.33
	2.12	12.78 ± 0.6
	3.34	26.94 ± 0.63
	5.54	41.08 ± 0.91
6.35	0.53	3.79 ± 0.1
	0.83	4.65 ± 0.22
	1.34	11.67 ± 0.54
	2.12	31.34 ± 0.82
	3.34	47.78 ± 0.76
	5.54	58.55 ± 1.06
7.74	0.53	4.4 ± 0.29
	0.83	6.21 ± 0.16
	1.34	16.39 ± 0.27
	2.12	38.35 ± 0.42
	3.34	53.52 ± 0.37
	5.54	62.64 ± 1.78
9.72	0.53	6.1 ± 0.27
	0.83	10.58 ± 0.12
	1.34	26.35 ± 0.32
	2.12	50.55 ± 0.36
	3.34	63.11 ± 0.64
	5.54	67.4 ± 0.53
11.56	0.53	7.96 ± 0.05
	0.83	15.17 ± 0.22
	1.34	34.6 ± 0.76
	2.12	58.47 ± 0.69
	3.34	69.41 ± 0.54
	5.54	71.67 ± 0.99

Table A.5: Subject 5 Deposition Data

Q (L/min)	d_a (μm)	η (%)
1.79	0.53	1.96 ± 0.92
	0.83	2.39 ± 1.51
	1.34	3.22 ± 1.65
	2.12	4.96 ± 0.96
	3.34	9.8 ± 0.25
	5.54	17.26 ± 0.16
3.14	0.53	2.13 ± 0.05
	0.83	2.67 ± 0.02
	1.34	4.97 ± 0.07
	2.12	13.89 ± 0.15
	3.34	30.12 ± 0.22
	5.54	45.41 ± 0.16
3.88	0.53	3.12 ± 0.25
	0.83	3.93 ± 0.33
	1.34	7.78 ± 0.32
	2.12	23.38 ± 0.52
	3.34	44.31 ± 1.41
	5.54	61.32 ± 1.08
6.12	0.53	4.79 ± 0.18
	0.83	7.11 ± 0.16
	1.34	19.2 ± 0.36
	2.12	48.03 ± 0.81
	3.34	66.23 ± 1.17
	5.54	75.54 ± 1.78
7.37	0.53	5.69 ± 0.11
	0.83	9.33 ± 0.16
	1.34	25.55 ± 0.3
	2.12	55.22 ± 0.9
	3.34	71.14 ± 1.22
	5.54	78.94 ± 1.67
9.40	0.53	8.19 ± 0.01
	0.83	15.14 ± 0.12
	1.34	38.07 ± 0.26
	2.12	67.07 ± 0.72
	3.34	78.64 ± 0.86
	5.54	81.08 ± 1.27
11.15	0.53	10.63 ± 0.06
	0.83	21.27 ± 0.11
	1.34	47.92 ± 0.25
	2.12	74.32 ± 0.48
	3.34	83.41 ± 0.51
	5.54	83.48 ± 0.55

Table A.6: Subject 7 Deposition Data

Q (L/min)	d_a (μm)	η (%)
1.77	0.53	1.98 ± 0.19
	0.83	2.28 ± 0.35
	1.34	2.84 ± 0.37
	2.12	4.93 ± 0.42
	3.34	9.23 ± 0.34
	5.54	18.04 ± 2.94
3.16	0.53	2.45 ± 0.32
	0.83	2.78 ± 0.22
	1.34	4.99 ± 0.21
	2.12	13.15 ± 0.13
	3.34	26.75 ± 0.06
	5.54	40.48 ± 0.07
4.07	0.53	2.75 ± 0.12
	0.83	3.35 ± 0.08
	1.34	7.42 ± 0.06
	2.12	20.63 ± 0.06
	3.34	36.19 ± 0.24
	5.54	51.4 ± 0.46
6.40	0.53	4.65 ± 0.3
	0.83	7.96 ± 0.54
	1.34	19.68 ± 0.91
	2.12	41.64 ± 0.42
	3.34	56.05 ± 0.19
	5.54	65.92 ± 0.33
7.86	0.53	5.49 ± 0.15
	0.83	11.09 ± 0.36
	1.34	26.55 ± 0.38
	2.12	49.03 ± 0.12
	3.34	61.8 ± 0.35
	5.54	69.16 ± 0.37
9.90	0.53	9.28 ± 0.38
	0.83	18.91 ± 0.65
	1.34	38.69 ± 0.44
	2.12	60.08 ± 0.2
	3.34	70.1 ± 0.29
	5.54	74.66 ± 0.27
11.59	0.53	12.82 ± 0.45
	0.83	26.19 ± 0.58
	1.34	47.82 ± 0.36
	2.12	67.32 ± 0.21
	3.34	75.64 ± 0.26
	5.54	78.5 ± 0.43

Table A.7: Subject 8 Deposition Data

Q (L/min)	d_a (μm)	η (%)
1.74	0.53	1.33 ± 0.09
	0.83	1.24 ± 0.09
	1.34	1.62 ± 0.06
	2.12	2.71 ± 0.23
	3.34	3.96 ± 0.51
	5.54	6.7 ± 1.21
3.37	0.53	1.52 ± 0.09
	0.83	1.33 ± 0.15
	1.34	1.43 ± 0.1
	2.12	2.48 ± 0.24
	3.34	4.96 ± 0.45
	5.54	10.09 ± 1.72
5.00	0.53	1.63 ± 0.21
	0.83	1.33 ± 0.19
	1.34	1.67 ± 0.19
	2.12	3.93 ± 0.2
	3.34	9.02 ± 0.42
	5.54	19.96 ± 1.76
7.67	0.53	1.45 ± 0.1
	0.83	1.28 ± 0.16
	1.34	2.56 ± 0.07
	2.12	7.95 ± 0.1
	3.34	17.75 ± 0.16
	5.54	32.4 ± 0.79
10.25	0.53	1.95 ± 0.23
	0.83	2.47 ± 0.18
	1.34	6.4 ± 0.03
	2.12	18.7 ± 0.13
	3.34	34.06 ± 0.43
	5.54	49.8 ± 0.83
13.08	0.53	2.27 ± 0.18
	0.83	3.75 ± 0.17
	1.34	10.64 ± 0.23
	2.12	28.04 ± 0.21
	3.34	44.54 ± 0.3
	5.54	56.15 ± 1.6
15.61	0.53	2.94 ± 0.06
	0.83	5.56 ± 0.07
	1.34	15.78 ± 0.18
	2.12	36.94 ± 0.46
	3.34	53.15 ± 0.35
	5.54	62.35 ± 0.17

Appendix B: Idealized Geometry Deposition Data

Table B.1: 0.6 Scale Deposition Data

Q (L/min)	d_a (μm)	η (%)
1.78	0.53	1.2 ± 0.18
	0.83	1.13 ± 0.26
	1.34	1.38 ± 0.24
	2.12	1.99 ± 0.33
	3.34	3.01 ± 0.35
	5.54	6.29 ± 0.58
3.16	0.53	1.52 ± 0.08
	0.83	1.47 ± 0.11
	1.34	1.74 ± 0.13
	2.12	3.48 ± 0.09
	3.34	8.7 ± 0.2
	5.54	20.83 ± 0.98
4.55	0.53	1.54 ± 0.18
	0.83	1.58 ± 0.19
	1.34	2.58 ± 0.18
	2.12	7.17 ± 0.2
	3.34	15.99 ± 0.32
	5.54	34.55 ± 0.31
6.80	0.53	2.69 ± 0.07
	0.83	3.22 ± 0.1
	1.34	6.97 ± 0.11
	2.12	16.75 ± 0.37
	3.34	30.49 ± 0.4
	5.54	50.9 ± 1.09
8.59	0.53	3.6 ± 0.09
	0.83	4.97 ± 0.16
	1.34	11.15 ± 0.46
	2.12	24.1 ± 0.83
	3.34	39.44 ± 1.04
	5.54	58.28 ± 1.91
10.84	0.53	5.01 ± 0.06
	0.83	7.93 ± 0.24
	1.34	17.4 ± 0.74
	2.12	34.38 ± 1.03
	3.34	49.93 ± 1.05
	5.54	63.3 ± 1.79
13.08	0.53	7.06 ± 0.58
	0.83	11.97 ± 1.25
	1.34	24.53 ± 2.14
	2.12	44.04 ± 2.24
	3.34	59.06 ± 1.53
	5.54	68.21 ± 1.63

Table B.2: 0.7 Scale Deposition Data

Q (L/min)	d_a (μm)	η (%)
--	0.53	--
	0.83	--
	1.34	--
	2.12	--
	3.34	--
	5.54	--
--	0.53	--
	0.83	--
	1.34	--
	2.12	--
	3.34	--
	5.54	--
4.53	0.53	1.69 ± 0.25
	0.83	1.78 ± 0.23
	1.34	2.64 ± 0.24
	2.12	6.44 ± 0.54
	3.34	14.57 ± 1.06
	5.54	29.65 ± 1.39
6.99	0.53	2.36 ± 0.17
	0.83	2.92 ± 0.19
	1.34	5.96 ± 0.26
	2.12	15 ± 0.55
	3.34	27.76 ± 1.25
	5.54	45.44 ± 0.96
8.76	0.53	3.45 ± 0.1
	0.83	4.82 ± 0.2
	1.34	10.49 ± 0.36
	2.12	23.09 ± 0.62
	3.34	37.82 ± 1.27
	5.54	54.65 ± 1.34
11.11	0.53	4.47 ± 0.29
	0.83	7.23 ± 0.47
	1.34	15.88 ± 0.64
	2.12	31.78 ± 0.77
	3.34	47.17 ± 0.79
	5.54	57.72 ± 0.39
13.43	0.53	5.65 ± 0.31
	0.83	9.93 ± 0.31
	1.34	21.5 ± 0.14
	2.12	39.6 ± 0.12
	3.34	55.23 ± 0.31
	5.54	63.25 ± 0.61

Table B.3: 0.8 Scale Deposition Data

Q (L/min)	d_a (μm)	η (%)
--	0.53	--
	0.83	--
	1.34	--
	2.12	--
	3.34	--
	5.54	--
--	0.53	--
	0.83	--
	1.34	--
	2.12	--
	3.34	--
	5.54	--
4.62	0.53	1.03 ± 0.12
	0.83	1.21 ± 0.15
	1.34	1.63 ± 0.52
	2.12	3.83 ± 0.4
	3.34	9.02 ± 0.41
	5.54	18.97 ± 1.19
6.87	0.53	1.9 ± 0.26
	0.83	2.19 ± 0.34
	1.34	3.67 ± 0.43
	2.12	9.08 ± 0.68
	3.34	19.23 ± 1.32
	5.54	32.97 ± 1.78
9.16	0.53	2.24 ± 0.14
	0.83	3.14 ± 0.18
	1.34	7.12 ± 0.38
	2.12	17.34 ± 0.74
	3.34	31.26 ± 1.56
	5.54	46.6 ± 2.1
11.68	0.53	3.57 ± 0.35
	0.83	5.43 ± 0.47
	1.34	12.04 ± 0.81
	2.12	25.4 ± 1.32
	3.34	40.88 ± 1.75
	5.54	51.74 ± 1.89
14.10	0.53	4.33 ± 0.28
	0.83	7.56 ± 0.51
	1.34	16.89 ± 0.88
	2.12	32.81 ± 1.25
	3.34	47.26 ± 3.53
	5.54	55.69 ± 3.6

Table B.4: Full Scale Deposition Data

Q (L/min)	d_a (μm)	η (%)
--	0.53	--
	0.83	--
	1.34	--
	2.12	--
	3.34	--
	5.54	--
--	0.53	--
	0.83	--
	1.34	--
	2.12	--
	3.34	--
	5.54	--
5.01	0.53	1.03 ± 0.21
	0.83	1.03 ± 0.17
	1.34	1.41 ± 0.18
	2.12	2.51 ± 0.18
	3.34	4.84 ± 0.12
	5.54	8.11 ± 0.63
7.62	0.53	0.85 ± 0
	0.83	0.95 ± 0.04
	1.34	1.57 ± 0.12
	2.12	3.61 ± 0
	3.34	8.12 ± 0.15
	5.54	16.02 ± 2.88
10.02	0.53	0.94 ± 0.26
	0.83	1.37 ± 0.24
	1.34	2.97 ± 0.28
	2.12	8.09 ± 0.39
	3.34	16.67 ± 0.19
	5.54	26.07 ± 0.87
12.68	0.53	1.53 ± 0.19
	0.83	2.15 ± 0.29
	1.34	4.76 ± 0.13
	2.12	12.25 ± 0.24
	3.34	22.22 ± 0.11
	5.54	30.72 ± 1.97
15.31	0.53	--
	0.83	--
	1.34	7.09 ± 0.38
	2.12	17.06 ± 0.3
	3.34	28.67 ± 0.13
	5.54	41.14 ± 4.49